



**NAVAL
POSTGRADUATE
SCHOOL**

MONTEREY, CALIFORNIA

THESIS

**HIGH ENERGY LASER APPLICATIONS IN A SURFACE
COMBATANT: TERMINAL PHASE THEATER
BALLISTIC MISSILE DEFENSE, LOW ATMOSPHERE
PROPAGATION, AND FREE ELECTRON LASER GAIN**

by

Sean P. Niles

June 2005

Thesis Advisor:
Second Reader:

William Colson
Robert Armstead

Approved for public release; distribution is unlimited

THIS PAGE INTENTIONALLY LEFT BLANK

REPORT DOCUMENTATION PAGE			Form Approved OMB No. 0704-0188	
Public reporting burden for this collection of information is estimated to average 1 hour per response, including the time for reviewing instruction, searching existing data sources, gathering and maintaining the data needed, and completing and reviewing the collection of information. Send comments regarding this burden estimate or any other aspect of this collection of information, including suggestions for reducing this burden, to Washington headquarters Services, Directorate for Information Operations and Reports, 1215 Jefferson Davis Highway, Suite 1204, Arlington, VA 22202-4302, and to the Office of Management and Budget, Paperwork Reduction Project (0704-0188) Washington DC 20503.				
1. AGENCY USE ONLY (Leave blank)		2. REPORT DATE June 2005	3. REPORT TYPE AND DATES COVERED Master's Thesis	
4. TITLE AND SUBTITLE: High Energy Laser Applications in a Surface Combatant: Terminal Phase Theater Ballistic Missile Defense, Low Atmosphere Propagation, and Free Electron Laser Gain			5. FUNDING NUMBERS	
6. AUTHOR(S) Niles, Sean P.				
7. PERFORMING ORGANIZATION NAME(S) AND ADDRESS(ES) Naval Postgraduate School Monterey, CA 93943-5000			8. PERFORMING ORGANIZATION REPORT NUMBER	
9. SPONSORING /MONITORING AGENCY NAME(S) AND ADDRESS(ES) N/A			10. SPONSORING/MONITORING AGENCY REPORT NUMBER	
11. SUPPLEMENTARY NOTES The views expressed in this thesis are those of the author and do not reflect the official policy or position of the Department of Defense or the U.S. Government.				
12a. DISTRIBUTION / AVAILABILITY STATEMENT Approved for public release; distribution is unlimited			12b. DISTRIBUTION CODE A	
13. ABSTRACT (maximum 200 words) The Free Electron Laser (FEL) can provide the naval surface combatant with a directed energy weapon that can be used against a large target set. Due to space constraints in a shipboard installation, an exploration is conducted to show the feasibility of short Rayleigh length FELs using a FEL simulation. Low atmosphere engagements are discussed through the modeling of a turbulence module for laser propagation in cruise missile defense applications. In particular, this thesis explores the difficulties in engaging a short/medium range theater ballistic missile (TBM) in the terminal phase as an engagement scenario in support of littoral operations using HELCoMES, developed by SAIC, as an engagement analysis tool. A concept of operations (CONOPS) for the use of a FEL as an area TBM defensive weapon is explored, using a unitary, high explosive warhead model and extrapolations to other TBM warhead types.				
14. SUBJECT TERMS Free Electron Laser, FEL, High Energy Laser, HEL, Low Current Gain, Turbulence, Atmospheric Propagation, Thermal Blooming, Theater Ballistic Missile Defense, TMBD, Terminal Phase			15. NUMBER OF PAGES 118	
			16. PRICE CODE	
17. SECURITY CLASSIFICATION OF REPORT Unclassified	18. SECURITY CLASSIFICATION OF THIS PAGE Unclassified	19. SECURITY CLASSIFICATION OF ABSTRACT Unclassified	20. LIMITATION OF ABSTRACT UL	

THIS PAGE INTENTIONALLY LEFT BLANK

Approved for public release; distribution is unlimited

**HIGH ENERGY LASER APPLICATIONS IN A SURFACE
COMBATANT: TERMINAL PHASE THEATER
BALLISTIC MISSILE DEFENSE, LOW ATMOSPHERE
PROPAGATION, AND FREE ELECTRON LASER GAIN**

Sean P. Niles
Lieutenant, United States Navy
B.N.E., Georgia Institute of Technology, 1997

Submitted in partial fulfillment of the
requirements for the degree of

MASTER OF SCIENCE IN APPLIED PHYSICS

from the

**NAVAL POSTGRADUATE SCHOOL
June 2005**

Author: Sean P. Niles

Approved by: William Colson
Thesis Advisor

Robert Armstead
Second Reader

James Luscombe
Chairman, Department of Physics

THIS PAGE INTENTIONALLY LEFT BLANK

ABSTRACT

The Free Electron Laser (FEL) can provide the naval surface combatant with a directed energy weapon that can be used against a large target set. Due to space constraints in a shipboard installation, an exploration is conducted to show the feasibility of short Rayleigh length FELs using a FEL simulation. Low atmosphere engagements are discussed through the modeling of a turbulence module for laser propagation in cruise missile defense applications. In particular, this thesis explores the difficulties in engaging a short/medium range theater ballistic missile (TBM) in the terminal phase as an engagement scenario in support of littoral operations using HELCoMES, developed by SAIC, as an engagement analysis tool. A concept of operations (CONOPS) for the use of a FEL as an area TBM defensive weapon is explored, using a unitary, high explosive warhead model and extrapolations to other TBM warhead types.

THIS PAGE INTENTIONALLY LEFT BLANK

DISCLAIMER

The computer programs in the Appendix are supplied on an “as is” basis, with no warranties of any kind. The author bears no responsibility for any consequences of using these program.

THIS PAGE INTENTIONALLY LEFT BLANK

TABLE OF CONTENTS

I.	INTRODUCTION	1
II.	HISTORY	3
	A. SYSTEM MAJOR COMPONENT DESCRIPTION	5
	B. FEL ATTRIBUTES	7
III.	FEL THEORY	11
	A. RELATIVISTIC LORENTZ EQUATIONS	11
	B. ELECTRON MOTION IN THE UNDULATOR	12
	C. MICROSCOPIC ELECTRON MOTION IN THE PRESENCE OF AN OPTICAL FIELD	14
	D. THE RESONANCE CONDITION	17
	E. ELECTRON PHASE, PHASE VELOCITY, AND DIMENSIONLESS OPTICAL FIELD	19
	F. SINGLE ELECTRON MOTION IN PHASE SPACE	19
	G. MOTION OF ELECTRONS IN PHASE SPACE	21
	H. COHERENCE CHARACTERISTICS	22
IV.	OPTICAL THEORY	25
	A. THE OPTICAL WAVE EQUATION	25
	B. PROPAGATION	29
	1. Scattering	29
	2. Absorption	31
	3. Thermal Blooming	33
	4. Turbulence	34
	C. COMPUTER MODELING	35
	1. Scattering and Absorption	35
	2. Thermal Blooming	36
	3. Turbulence	40

V.	SHORT RAYLEIGH LENGTH SYSTEMS	49
A.	SIZE CONSTRAINTS	49
B.	OPTICAL DAMAGE	50
C.	GAIN THEORY	51
VI.	THEATER BALLISTIC MISSILE DEFENSE	55
A.	CURRENT STATUS	55
1.	Sensor Networks	56
2.	Weapons	57
B.	DAMAGE REQUIREMENTS	57
1.	Missile Models	59
2.	Flight Patterns	59
3.	Damage Methodologies	60
4.	TBMD Scenarios	64
C.	CONCEPT OF OPERATIONS FOR TMBD LASER	71
1.	Engagement Criteria	71
2.	Self-Defense Considerations	73
3.	Area Defense Considerations	73
4.	Weapon Readiness Conditions	74
D.	ADDITIONAL BENEFITS	75
1.	Optical Uses	76
2.	Sea Skimming Cruise Missile Defense	76
3.	Small Craft Swarm Defense	77
VII.	CONCLUSION	79
	APPENDIX A. CODE	81
1.	WAVE PROPAGATION CODE	81
2.	BEAM ANALYSIS	95
	LIST OF REFERENCES	97
	INITIAL DISTRIBUTION LIST	99

LIST OF FIGURES

1.	An Example of an Accelerator Based FEL	5
2.	A Simplified Diagram of a Photo-Cathode Electron Gun	5
3.	A Superconducting RF Cavity	6
4.	A Longitudinal Undulator	7
5.	Magnetic Fields in a Helical Undulator	12
6.	Single Electron Paths	20
7.	Typical FEL Beam Phase Space	22
8.	Rayleigh and Mie Scattering Radiation Patterns	30
9.	Atmospheric Transmittance at Sea Level	32
10.	Various Atmospheric Absorption Profiles	36
11.	Various Atmospheric Scattering Profiles	36
12.	Propagating Beam – No Blooming	38
13.	Propagating Beam – Mild Blooming	38
14.	Propagating Beam – Moderate Blooming	39
15.	An Extended Turbulent Medium	40
16.	Multiple Phase Screens Used to Simulate an Extended Turbulent Medium	41
17.	Beam Wander, Broadening, and Scintillation	42
18.	Kolmogorov Power Spectral Density	43
19.	Phase Screen Generation Process	44
20.	Example Phase Screens	45
21.	Large Scale Turbules – Beam Wander	46
22.	Small Scale Turbules – Beam Breakup and Spreading	47
23.	C_n^2 as a Function of ϕ_t	48
24.	Gain for Various Rayleigh Ranges and Currents	54
25.	nominal TBM flight paths	61
26.	TBMD Engagement Geometry Scenarios	65

27.	Midlatitude Summer Navy, 14.8 km Visibility Profile	68
28.	Clear 2 Wind Profile	69
29.	Maritime Hufnagle-Valley 5/7 Turbulence Profile	70

LIST OF TABLES

I.	Types of Atmospheric Scattering	29
II.	TBMD Weapons	58
III.	Medium and Short Range TBMs	59
IV.	Material Dependent Spot Size for $10 \text{ kW/cm}^2 \mathcal{I}_0$	63
V.	Fluence Requirements and Melt-Through Times for Various 1 cm Slabs	64
VI.	Scenario Fluence Requirements	66
VII.	Fast TBM Intercept Results	69
VIII.	Slow TBM Intercept Results	70

THIS PAGE INTENTIONALLY LEFT BLANK

ACKNOWLEDGMENTS

Many people have been helpful in the preparation of this thesis. First and foremost are my wife, Cheryl, and daughter, Lindsey. I appreciate the understanding and opportunities for tickle fights to relieve the stress of school. I can't wait for the day that I can explain all of this to you Lindsey.

I would also like to thank the professors that inspired me and assisted me in my many times of needs: Professor Colson for the "Colsonian" that for all my good natured ribbing really did make my thesis much better. Professor Armstead for his patience in having to read 10-20 pages of theory at a time and for the much needed pointers in developing a coherent derivation. Professors Blau (aka. "Joe Slide") and Crooker for comic relief and never ending prodding to get the physics correct. Professor Borden for his ability to make me laugh even as he handed back a disastrous test – I also appreciate the opportunities to vent with immunity and the numerous "reality checks" as they were required. To the other professors I encountered at NPS, I can say that I did not meet a single one that was not professional or determined to do their best for the students in their charge. Thank you for challenging me.

To the guys in the FEL office...what can I say? Brett, you're a trip and a half. I can't believe you actually understand all that math stuff that they threw at us, but it certainly came in handy when the rest of us needed something translated down to our level. Robb, you continue my streak of meeting Marine officers that I admire and aspire to pattern myself after. Oscar, your determination is legendary – and I hope that all goes well for you in the future. To the new guys, good luck! Stick together and HAVE FUN! To the "Go Time" crew, MuaDib is retiring...I would leave you my cheat codes, but I forgot them already!

THIS PAGE INTENTIONALLY LEFT BLANK

I. INTRODUCTION

As the Navy continues to embrace new technology to assist in its fight at sea, new weapons must be considered for a growing number of roles. Directed energy, in the form of high energy lasers and rail guns, will allow the projection of power over a much greater range and in less time than previously capable. However, our enemies continue to amass weapons with the capability to reach further out to sea, placing our ships in danger of attack.

The free electron laser shows promise as a directed energy weapon aboard ship. It will provide the ability to engage a vast target set including sea skimming cruise missiles and theater ballistic missiles. For any shipboard installation, a weapon system must fit into the constraints imposed in modern shipbuilding and must show a high return (i.e. effectiveness) on the money invested in its development and installation. The free electron laser, in a short Rayleigh length configuration, could fit within the confines of current watertight bulkhead layout with sufficient output power for weapon applications. The Navy is already moving toward a high energy laser solution to counter low altitude cruise missiles; with a moderate upgrade in power over the output power levels currently under consideration, a high energy laser could be used for theater ballistic missile defense as well.

This thesis investigates the attributes of the free electron laser and how those attributes make it an ideal candidate for use as a ship self-defense weapon. Additionally, a study is conducted describing a wave propagation code and atmospheric effect modules that can be used to represent atmospheric phenomena, including thermal blooming and turbulence. Finally, a study is conducted in the application of a high energy laser as a terminal phase theater ballistic missile defense weapon. From the positive results showing that such a laser can be successful in a self-defense mode, some basic concepts of operation are explored.

THIS PAGE INTENTIONALLY LEFT BLANK

II. HISTORY

The Free Electron Laser (FEL) is the culmination of many years of development in coherent radiation sources. Beginning with microwave tubes in the 1930's, scientists and engineers realized they could generate coherent radiation from microwave cavities using a beam of electrons. They later developed the open resonator that allowed them to collect the radiation from bound electron transitions. Finally, combining the technologies from microwave tubes and the open resonator, it was realized that coherent radiation from free electrons could be created at arbitrary wavelengths.

In a microwave tube, the wavelength of radiation that is generated depends on the size of the resonant cavity. If the cavity is 5 cm across, then the light that is stored has a wavelength of about 5 cm. As the technology has matured, wall plug efficiencies have reached 60%. Microwave tubes have been unable to achieve shorter optical wavelengths because the cavities cannot be made small enough.

To generate coherent radiation at short wavelengths, scientists turned to other means. Atomic and molecular lasers were the next major development. “Laser” is an acronym standing for “light amplification by stimulated emission of radiation”. Scientists were able to “pump” bound electrons in certain materials into excited states. Then, through the cascade of the electrons into lower energy states, photons are emitted with a characteristic wavelength that is derived from the energy difference between the two energy states. The development of the optical resonator enabled the process to work effectively. A common characteristic of all atomic and molecular lasers is that they require some lasing medium for the process to take place. Whether the lasing medium is a gas, solid crystalline structure, or a liquid, the lasing process is essentially the same. Some material is placed in the optical resonator, and bound electrons are pumped to higher energy states and allowed to cascade to a lower state. The radiation that is generated by these devices can be powerful enough to burn through steel. Devices can be designed and built for many wavelengths of light and

output powers. However, these lasers are not continuously tunable over a significant range of wavelengths. When high power applications are considered, all solid state lasers suffer from heat dissipation issues. The lasing medium must withstand several times the amount of output power for the duration of the application. The heat that is generated in the lasing medium must be dissipated, otherwise the lasing medium will fail.

In the 1970's, it was hypothesised that a laser could be developed that did not require atoms in the lasing medium. Instead of pumping bound electrons and allowing them to change states, a beam of "free" electrons could be used. Particle accelerators were in widespread use, and provided an ample supply of non-bound (free) electrons that could be used to test this theory. In a FEL, a beam of free electrons is passed through a periodic magnetic field. The Lorentz force causes the electron beam to deflect slightly. This acceleration causes the electrons to radiate synchrotron radiation. By careful design, the electrons can be made to radiate coherently as they pass through the magnetic field. When this process is surrounded by an optical resonator or used to amplify another laser beam, the optical fields can be built up to high power and used for many purposes. The FEL is not subject to the heat build up of atomic and molecular lasers as the lasing medium (the electron beam) moves through the lasing cavity at nearly the speed of light and carries away the enthalpy deposited in the electron beam from the lasing interaction. Also, the FEL is not tied to a characteristic wavelength associated with a particular lasing medium. FELs can be designed to operate over a wide spectrum of wavelengths, from microwaves to x-rays, based upon the energy of the electron beam and the amplitude and period of the magnetic field. A FEL, once built, can change its wavelength by as much as an order of magnitude.

A. SYSTEM MAJOR COMPONENT DESCRIPTION

A FEL can be designed around almost any electron accelerator or device that circulates or accelerates a relativistic electron beam. Most FELs are designed to be used with electron accelerators as shown in Figure (1).

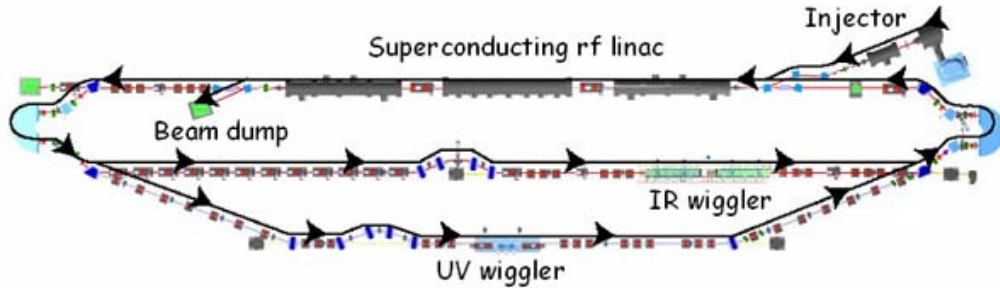


Figure 1. An example of an accelerator based FEL [1]

The first major piece of equipment of the electron beam path is the photocathode, as shown in Figure(2). The photocathode uses the photoelectric effect to extract bunches of electrons from a metal surface. This is accomplished using another laser that supplies the necessary energy to eject a number of electrons from the metal lattice into free space. Inside the injector's housing, a high voltage is maintained that accelerates any electrons released from the metal away from the cathode surface.

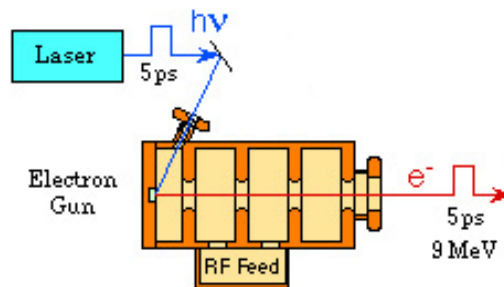


Figure 2. A simplified diagram of a photo-cathode electron gun

After the electron gun, the electron bunches are accelerated using standard electron accelerator modules. FELs have been designed around both copper radio frequency (RF) cavities and superconducting RF modules. Accelerating cavities have many configurations, but Figure (3) shows what a superconducting RF cavity looks like outside of its cryomodule. Depending on the beam energy desired, multiple accelerator modules can be used to increase the kinetic energy of the electrons. The remainder of the beam path consists of magnets that adjust the geometry of the electron bunch and move the electrons through the beam pipe to the undulator.

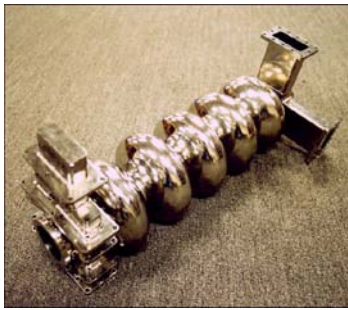


Figure 3. Superconducting RF cavity produced by Jefferson Labs[2].

The undulator is the first piece of equipment that is unique to the laser portion of the machine. An undulator is a device that contains a periodic, transverse magnetic field that causes the electron bunches to accelerate due to the Lorentz force. Two major types are used, helical and longitudinal. Helical undulators cause the electrons to follow a helical path through the interior of the undulator. Longitudinal undulators (see Figure (4)) have an alternating magnetic field oriented perpendicular to the electron beam path. As the electrons pass through the undulator, they follow a sinusoidal path, wiggling in the direction perpendicular to both the magnetic field and beam path. The motion of the electrons causes them to radiate in the forward direction. Some of this light is then collected in the optical resonator.

The optical resonator is a set of mirrors that allow the some of the light radiated from the electrons to bounce back and forth and remain within the system.

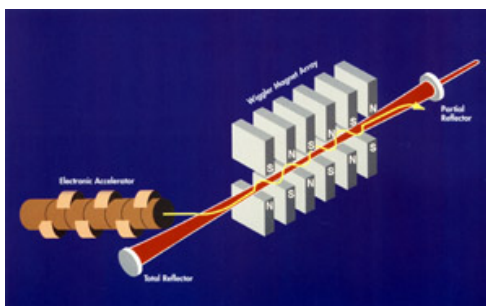


Figure 4. A longitudinal undulator[3].

Of the two mirrors, one is highly reflecting and one is partially transmissive. The light that transmits through the partial mirror is the output light that is used for applications. Also, by allowing the light to reflect back and forth in the resonator, it provides a light field with which the electrons passing through the undulator can interact. Through this interaction, the electrons “bunch”, which causes them to radiate coherently. This coherent radiation is the lasing mechanism for the FEL.

In some FELs, the electron beam is not dumped immediately after the undulator. The electrons still retain much of the kinetic energy they acquired as they passed through the accelerator. By passing the same electron bunches through the accelerating modules, but out of phase with the RF field, the electrons can be induced to give up their kinetic energy to the RF fields, essentially recycling their energy to the next bunch injected from the photocathode. This process serves two purposes, increasing the efficiency of the overall machine, and reducing the energy of the electrons that are sent to the beam dump. By reducing the energy of the dumped electrons, recirculation decreases the induced radioactivity of the target material.

B. FEL ATTRIBUTES

FELs are large, complex machines. The electron beam path must be large enough to allow for the necessary accelerating modules to reach the required kinetic energy. In a high power design, the optical resonator must be long enough to allow the

optical fields to expand enough to reduce the incident intensity on the mirrors below the damage threshold for the component material. Because the system is composed of many high tolerance, exotic, and expensive materials, the overall cost is fairly high. The system is electrically driven, and its power requirements for lasing are somewhat high. However, when not actively lasing, the maintenance system draw is stable and much lower than the lasing requirement.

On the positive side, FELs are unique in the combination of reliability, tunability, and efficiency they bring to an application. FEL systems have demonstrated continuous lasing for months. Many high power lasers are unable to maintain their design power for even a few seconds due to lasing medium heat dissipation constraints. FELs, with a continuously refreshed lasing medium to capture heat, can operate as long as the attached electron accelerator can provide electron bunches to maintain lasing in the optical resonator, and have been demonstrated to maintain lasing for several days. Once an electron beam accelerator is established, numerous FEL designs can be implemented on the same machine. All that is necessary is a beam path to the undulator and associated resonator, and a path to return the electrons to the accelerator's beam path for recirculation, if desired. By recirculating the electron beam after the undulator, a FEL can achieve conservative efficiencies above 10%. Within a given design, a FEL can be tuned to a desired wavelength within approximately one order of magnitude from the designed wavelength, simply by adjusting the electron beam energy. Atomic and molecular lasers are unable to change their wavelength beyond the characteristic wavelengths of the lasing medium. If an application calls for another wavelength, another laser must be used or designed.

Overall, FELs cannot yet match atomic and molecular lasers in raw output power. However, they are close. The Thomas Jefferson National Accelerator Facility recently achieved 10 kW output power [8]. The benefits of higher efficiency, designability throughout the electromagnetic spectrum, tunability in the same laser, and greater reliability give them a firm footing for potential use in many applications. As

the upper boundary in output power for FELs is pushed higher, their implementation in the face of extra size and cost becomes much easier to justify.

THIS PAGE INTENTIONALLY LEFT BLANK

III. FEL THEORY

A. RELATIVISTIC LORENTZ EQUATIONS

In order to generate light, a beam of electrons must experience a field that accelerates them. In a FEL, the accelerating force is in the form of a periodic magnetic field, formed by a device called the undulator or wiggler. Because the electrons are relativistic, with $v \approx c$, the radiation generated is focused primarily along the direction of electron motion. In order to determine how this radiation is generated, it is necessary to understand the forces on the electrons. The motion of electrons in the presence of a magnetic field is governed by the Lorentz Force equations. Once radiation (“light”) is present, the alternating electromagnetic fields in the optical field change the motion of the electrons.

The Lorentz force equation governs the motion of charged particles exposed to a magnetic field,

$$\mathbf{F} = q \left(\mathbf{E} + \frac{\mathbf{v}}{c} \times \mathbf{B} \right) = \frac{d\mathbf{p}}{dt} \quad . \quad (\text{III.1})$$

For the FEL, $q = -e$, and the Lorentz force may be written with the corresponding energy (γmc^2) changes,

$$\frac{\mathbf{F}}{mc} = \frac{-e}{mc} (\mathbf{E} + \boldsymbol{\beta} \times \mathbf{B}) = \frac{d(\gamma\boldsymbol{\beta})}{dt} \quad , \quad (\text{III.2})$$

$$\frac{d\gamma}{dt} = \frac{-e}{mc} (\boldsymbol{\beta} \cdot \mathbf{E}) \quad . \quad (\text{III.3})$$

In Equations (III.1), (III.2), and (III.3), $-e$ is the charge on the electron, m is the rest mass of the electron, \mathbf{v} is electron velocity, $\boldsymbol{\beta} = \mathbf{v}/c$ is the relativistic electron velocity, c is the speed of light, t is time, \mathbf{E} is the electric field, \mathbf{B} is the magnetic field, and γ is the Lorentz factor, $\gamma = (1 - \beta^2)^{-\frac{1}{2}}$.

To further develop the equations, we define a specific magnetic field, in this case, a helical field. A constant magnitude helical field can be described by Equation (III.4), in which there is no magnetic field component in the axis (z) direction. Figure

(5) shows how the fields in a helical undulator change with position down the axis,

$$\mathbf{B} = B (\cos (k_0 z), \sin (k_0 z), 0) \quad . \quad (\text{III.4})$$

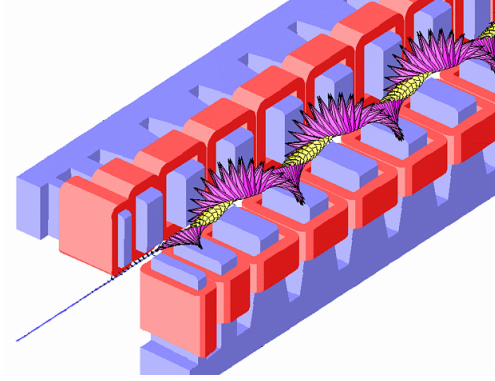


Figure 5. A diagonal slice cut away of a helical undulator showing the rotating magnetic field as a function of position along the undulator axis[4]

For the FEL, the only \mathbf{E} fields present are those due to light within the FEL resonator. Since the electrons are accelerated by a static helical magnetic field, it is natural that the light generated is helically polarized. The changing \mathbf{E} field of the optical beam has associated with it a changing \mathbf{B} field, and both are described by Equations (III.5, III.6, III.7). We assume that the light present is in the form of a plane wave,

$$\mathbf{E}_s = E (\cos \psi, -\sin \psi, 0) \quad , \quad (\text{III.5})$$

$$\mathbf{B}_s = E (\sin \psi, \cos \psi, 0) \quad , \quad (\text{III.6})$$

$$\psi \equiv kz - \omega t + \phi \quad . \quad (\text{III.7})$$

B. ELECTRON MOTION IN THE UNDULATOR

Using Equations (III.5, III.6, III.7) and assuming that there is no light in the FEL, we now solve for the actual motion of the electrons under the influence of the helical magnetic field. Even in the presence of light, the transverse motion of the electrons is determined by the undulator field.

Equation (III.3) tells us that the small change in the electron energy is proportional to the dot product between the electric field of the light and the velocity of the electron. Since there is no light present, then the electric field is zero and γ is constant. Using this knowledge in Equation (III.2), we find the following equation of motion,

$$\frac{d\boldsymbol{\beta}}{dt} = \frac{-e}{\gamma mc} (\boldsymbol{\beta} \times \mathbf{B}) \quad . \quad (\text{III.8})$$

Putting \mathbf{B} from Equation (III.4) into Equation (III.8) yields

$$\frac{d\boldsymbol{\beta}}{dt} = \frac{-eB}{\gamma mc} (-\beta_z \sin(k_0 z), \beta_z \cos(k_0 z), \beta_x \sin(k_0 z) - \beta_y \cos(k_0 z)) \quad . \quad (\text{III.9})$$

We can observe that the x and y components are different only by a $\pi/2$ phase shift. This means the motion is the same in both $\hat{\mathbf{x}}$ and $\hat{\mathbf{y}}$ directions, only shifted in time or space. Solving for the transverse motion, we find that

$$\boldsymbol{\beta}_\perp = \frac{-eB\lambda_0}{2\pi\gamma mc^2} (\cos(k_0 z), \sin(k_0 z), 0) \quad (\text{III.10})$$

assuming the constants of integration are zero, indicating perfect injection into helical orbits. Substitution of Equation (III.10) into Equation (III.9) shows that for perfect helical orbits, $\dot{\beta}_z = 0$, with the solution $z = \beta_z ct$.

Now, define the undulator parameter as $K = eB\lambda_0/2\pi mc^2$. Performing this substitution, the transverse electron motion is

$$\boldsymbol{\beta}_\perp = \frac{-K}{\gamma} (\cos(k_0 z), \sin(k_0 z), 0) \quad . \quad (\text{III.11})$$

For relativistic electrons $\beta_z \simeq 1$, so that

$$z(t) = \beta_z ct \simeq ct \quad . \quad (\text{III.12})$$

This gives

$$\begin{aligned} k_0 z &\simeq k_0 ct \quad , \\ k_0 z &\simeq \omega_0 t \quad . \end{aligned} \quad (\text{III.13})$$

Substituting this into (III.11), we find the perpendicular motion of the electrons is described by

$$\boldsymbol{\beta}_{\perp} \simeq \frac{\mathbf{v}_{\perp}}{c} \simeq \frac{-K}{\gamma} (\cos(\omega_0 t), \sin(\omega_0 t), 0) \quad . \quad (\text{III.14})$$

If we integrate (III.14) and use the substitution $c/\omega_0 = 1/k_0 = \lambda_0/2\pi$, we can find the trajectories of the electrons' transverse components

$$\mathbf{x}_{\perp} \simeq \frac{K\lambda_0}{2\pi\gamma} (-\sin(\omega_0 t), \cos(\omega_0 t), 0) \quad . \quad (\text{III.15})$$

Now that we have an equation for the motion of the electrons as they pass through a helical undulator, it would be instructive to know some magnitudes of the electron deviations. If we use typical parameters, $K \sim 1$, $\gamma \sim 100$, $\lambda_0 \sim 5\text{cm}$, we find the electrons only oscillate in the transverse directions by $|x_{\perp}| \sim 100\mu\text{m}$. Compared to a typical electron beam size that is $\sim 1\text{ mm}$ in diameter, the electron deviation is very small. Using the same parameters, we can find the maximum $\mathbf{v}_{\perp} \approx Kc/\gamma$, from Equation (III.14). The magnitude is $v_{\perp} \approx 0.01c$ and is small compared to the velocity in the z direction down the oscillator axis. Another interesting question is the time necessary to complete an electron's oscillation, which is the period of oscillation, $\mathcal{T} = 2\pi/\omega_0 = \lambda_0/c \approx 167\text{ fs}$, from either of Equations (III.14) or (III.15).

C. MICROSCOPIC ELECTRON MOTION IN THE PRESENCE OF AN OPTICAL FIELD

Having considered the simplified case where no optical fields are present in the undulator, let us now consider the addition of a plane wave optical field that is helically polarized. Such a field can be described by the vector Equations (III.5, III.6, III.7), reproduced below,

$$\mathbf{E}_{\mathbf{s}} = E (\cos \psi, -\sin \psi, 0) \quad , \quad (\text{III.5})$$

$$\mathbf{B}_{\mathbf{s}} = E (\sin \psi, \cos \psi, 0) \quad , \quad (\text{III.6})$$

$$\psi \equiv kz - \omega t + \phi \quad . \quad (\text{III.7})$$

Following the same derivation procedure as before, and obtain the following equations for the electron transverse motion

$$\frac{d(\gamma\boldsymbol{\beta}_\perp)}{dt} = \frac{-e}{mc} [E(1 - \beta_z)(\cos\psi, -\sin\psi, 0) + \beta_z B(-\sin(k_0z), \cos(k_0z), 0)] \quad . \quad (\text{III.16})$$

For relativistic electrons $\beta_z \simeq 1$, and the optical field term proportional to \mathbf{E} can be ignored to first order, leaving us with the previous equation for the perpendicular motion, given by (III.11). Equation (III.17) describes how the energy of an electron changes with respect to time,

$$\frac{d\gamma}{dt} = \frac{-e}{mc} (\boldsymbol{\beta} \cdot \mathbf{E}) = \frac{-eE}{mc} (\beta_x \cos\psi - \beta_y \sin\psi) \quad . \quad (\text{III.17})$$

The longitudinal equation of motion,

$$\frac{d(\gamma\beta_z)}{dt} = \frac{-e}{mc} [E(\beta_x \cos\psi - \beta_y \sin\psi) + B(\beta_x \sin(k_0z) - \beta_y \cos(k_0z))] \quad , \quad (\text{III.18})$$

can be ignored because we have 5 equations using $\gamma = (1 - \beta^2)^{-1/2}$ and only 4 unknowns x, y, z , and γ . We now substitute the equations for β_x and β_y into Equation (III.17) to obtain

$$\dot{\gamma} = \frac{eKE}{\gamma mc} (\cos(k_0z) \cos\psi - \sin(k_0z) \sin\psi) = \frac{eKE}{\gamma mc} \cos(k_0z + \psi) \quad . \quad (\text{III.19})$$

If we now define the electron phase $\zeta = (k + k_0)z - \omega t$, then $k_0z + \psi = \zeta + \phi$, so that

$$\dot{\gamma} = \frac{eKE}{\gamma mc} \cos(\zeta + \phi) \quad . \quad (\text{III.20})$$

This looks almost like the pendulum equation, since γ and ζ are related. To get to the pendulum equation, we relate $\dot{\gamma}$ to $\ddot{\zeta}$, through

$$\gamma^{-2} \equiv 1 - \beta_z^2 - \beta_\perp^2 = 1 - \beta_z^2 - \frac{K^2}{\gamma^2} \quad ,$$

so that

$$\beta_z^2 = 1 - \frac{1 + K^2}{\gamma^2} \quad ,$$

and,

$$\beta_z = 1 - \frac{1 + K^2}{2\gamma^2} \quad \text{for } \gamma \gg 1 \quad \text{and} \quad K \approx 1. \quad (\text{III.21})$$

The derivative of the electron phase is

$$\begin{aligned} \dot{\zeta} &= (k + k_0) \dot{z} - \omega, \\ &= (k_0 + k) \beta_z c - \omega, \quad \text{and} \\ &= kc \left(1 - \frac{1 + K^2}{2\gamma^2} \right) - \omega, \quad \text{since } k \gg k_0. \end{aligned} \quad (\text{III.22})$$

Thus,

$$\begin{aligned} \ddot{\zeta} &= kc \left(\frac{1 + K^2}{2\gamma^2} \right) \left(\frac{2\dot{\gamma}}{\gamma} \right), \\ &= \dot{\gamma} kc \frac{1 + K^2}{\gamma^3}, \quad \text{where we have used III.20, so that} \\ \ddot{\zeta} &= \frac{2eEKk_0}{\gamma^2 m} \cos(\zeta + \phi). \end{aligned} \quad (\text{III.23})$$

If we define the dimensionless time τ as the time required for light to traverse the undulator, then $\tau \equiv ct/L = 0 \rightarrow 1$, from the beginning to the end of the undulator. This gives us a dimensionless measure of time that we can use in our determination of the evolution of the electron phase, since the relativistic electrons and light are traveling at near the same speed $\beta_z c \approx c$. We then have

$$\begin{aligned} \overset{\circ}{\zeta} &\equiv \frac{d^2\zeta}{d\tau^2} = \frac{d^2\zeta}{dt^2} \frac{c^2}{L^2}, \\ &= \frac{2eEKk_0L^2}{\gamma^2 mc^2} \cos(\zeta + \phi). \end{aligned} \quad (\text{III.24})$$

If we define the coefficient in front of the cosine term as the dimensionless optical field amplitude, $|a|$, we have derived the pendulum equation for the microscopic motion of the electrons in the undulator in the presence of an optical field,

$$\overset{\circ}{\zeta} = |a| \cos(\zeta + \phi). \quad (\text{III.25})$$

D. THE RESONANCE CONDITION

Proceeding, we develop some of the properties of the dimensionless electron phase velocity, $\nu = \dot{\zeta}$. Recall that

$$\begin{aligned}\dot{\zeta} &= \frac{L}{c} \dot{\zeta} \quad \text{and} \\ \dot{\zeta} &= (k + k_0) v_z - \omega \quad .\end{aligned}$$

Thus,

$$\nu = L [(k + k_0) \beta_z - k] \quad . \quad (\text{III.26})$$

Substituting Equation (III.21) for β_z ,

$$\nu = L \left[k \left(1 - \frac{1 + K^2}{2\gamma^2} \right) + k_0 \left(1 - \frac{1 + K^2}{2\gamma^2} \right) - k \right] \quad ,$$

and ignoring terms higher order terms of order k_0/γ^2 ,

$$\nu = L \left[k_0 - \frac{k(1 + K^2)}{2\gamma^2} \right] \quad . \quad (\text{III.27})$$

If, at this point, the phase velocity is set to zero ($\nu = 0$), then the electrons will take as much energy back from the light field as they give it, resulting in zero net energy exchange. This situation is known as the ‘‘resonance condition’’. Using Equation (III.27),

$$k_0 = k \frac{1 + K^2}{2\gamma^2} \quad ,$$

and

$$\lambda = \lambda_0 \frac{1 + K^2}{2\gamma^2} \quad . \quad (\text{III.28})$$

Equation (III.28) relates the wavelength of the undulator, λ_0 , to the wavelength of output light, λ .

To observe how the electron energy changes the electron phase velocity, we start from Equation (III.27). Taking the derivative relative to γ ,

$$\begin{aligned}\frac{d\nu}{d\gamma} &= L \left[0 - \frac{k(1 + K^2)}{2} \left(\frac{-2}{\gamma^3} \right) \right] \quad , \\ &= \frac{Lk(1 + K^2)}{\gamma^2} \frac{d\gamma}{\gamma} \quad .\end{aligned} \quad (\text{III.29})$$

Substituting $L = N\lambda_0$, $k = 2\pi/\lambda$, and the resonance Equation (III.28) into the above equation, it simplifies substantially

$$\begin{aligned} d\nu &= \frac{2\pi N\lambda_0(1+K^2)}{\lambda\gamma^2} \frac{d\gamma}{\gamma} \ , \\ &= 4\pi N \frac{d\gamma}{\gamma} \ . \end{aligned} \tag{III.30}$$

Thus, we see how changing the electron beam energy results in a change in the phase velocity. Using numerical values to get a sense of how a one percent change in the beam energy will affect the phase velocity, if $\gamma = 100$ and $N = 20$, we see that the phase velocity changes by $d\nu \approx 2.5$.

To observe the change in output wavelength as a function of beam energy, we return to the resonance condition (III.27). Taking the derivative of ν with respect to λ yields,

$$d\nu = \frac{-L(1+K^2)}{2\gamma^2} dk \ .$$

Since $k = 2\pi/\lambda$, we have $dk = -2\pi d\lambda/\lambda^2$, so that

$$\begin{aligned} d\nu &= \frac{-L(1+K^2)}{2\gamma^2} \left(\frac{-2\pi d\lambda}{\lambda^2} \right) = \left(\frac{\lambda_0(1+K^2)}{2\gamma^2} \right) 2\pi N \frac{d\lambda}{\lambda^2} \ . \\ d\nu &= 2\pi N \frac{d\lambda}{\lambda} \ . \end{aligned} \tag{III.31}$$

We find that an incremental change of electron beam energy, $d\gamma$, and an incremental change of the optical wavelength, $d\lambda$ affect the electron phase velocity as

$$d\nu = 4\pi N \frac{d\gamma}{\gamma} = 2\pi N \frac{d\lambda}{\lambda} \ . \tag{III.32}$$

Interpreting Equation (III.30) as before, and using the resulting phase velocity change in Equation (III.32) indicates that the previous 1% change in beam energy results in a change in the wavelength of 2%. This result indicates that the FEL's output wavelength is fairly sensitive to small changes in the beam parameters. However, it would not be desirable for the beam wavelength to vary due to small inconsistencies in the input electron beam. It also shows that the output beam is tunable over some

wavelength range depending on the ability of the electron source to provide electrons of the appropriate energy. The tunability is further constrained by the mirrors that are used.

E. ELECTRON PHASE, PHASE VELOCITY, AND DIMENSIONLESS OPTICAL FIELD

Using phase space, we can describe the motion of the electrons as a combination of their phase, ζ , and their phase velocity, $\nu = \dot{\zeta}$. The phase can be looked at as the “position” of the electron in its oscillatory orbit relative to a wavelength of light, while the phase velocity can be seen as the rate at which the electron’s phase is changing. The phase velocity of a particular electron is the rate and direction at which the phase between that electron and an associated light wave are changing. When ν increases, this indicates an electron is gaining energy from the optical field, while if ν decreases, it indicates the electron is giving energy to the optical field. The dimensionless optical field $|a|$ is a measure of the strength of the optical field and relates to the size of the path in (ζ, ν) (called the separatrix) which separates open and closed orbits of the pendulum motion. When speaking of dimensionless optical fields, two primary regimes are described: weak fields are described by $|a| \leq \pi$, and strong fields are described by $|a| > \pi$.

F. SINGLE ELECTRON MOTION IN PHASE SPACE

If we desire to discuss how a single electron moves about in phase space, we can approximate its motion as that of a simple pendulum. To illustrate this, Figure (6) shows the paths of several individual electrons in phase space. We can see that electrons that are inside the separatrix (black path) remain inside the separatrix and orbit over closed paths. Those electrons that are outside the separatrix have open paths. In the open path regions, the electrons cannot change the sign of their phase velocity as the closed path electrons do. This means that an electron, in an open orbit, that starts with a positive ν cannot be found in the region of $-\nu$ at some later

time if the field strength does not change. In open orbits, the ν value can decrease however, as discussed later. The height of the separatrix is given by $2\sqrt{|a|}$.

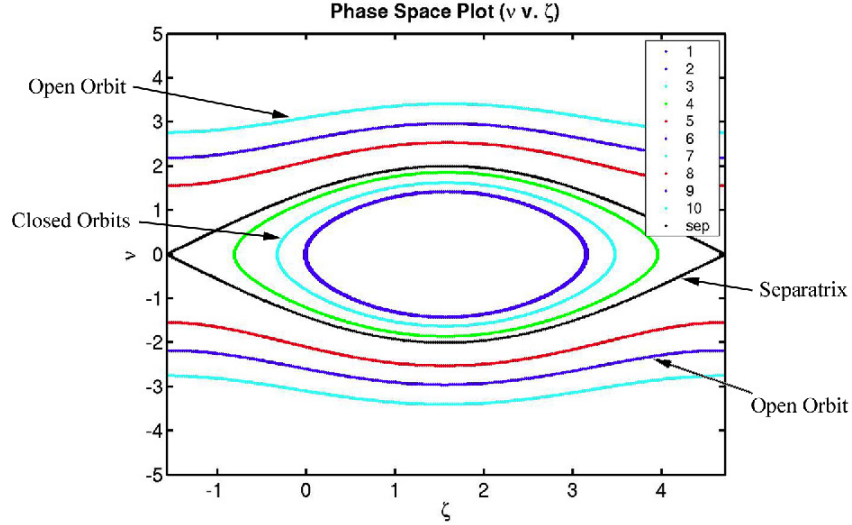


Figure 6. Ten phase-space paths represented by simple pendula. All were started with $\zeta = 0$ and varying ν values. The separatrix is drawn as well using open loop orbits approaching closed orbits. Periodic boundary conditions are used at $-\pi/2$ and $3\pi/2$.

The phase space plots also allow us to see the energy transfer between the electrons and the optical fields. The strength of the optical field determines the height of the separatrix ($2\sqrt{|a|}$). If there is a spread in the ν of the electrons, this means that in weak fields only electrons near resonance ($\nu = 0$) will be in closed orbits. As the optical field gains strength and expands the separatrix, more electrons are then found in closed orbits. In order to achieve beneficial energy transfer, we desire that the electrons lose energy to the optical field. This is represented in phase space by the electrons moving to a lower ν . In Figure(6), the electrons lower their energy most rapidly near the point $\zeta \approx \pi$ since the electrons' orbits are downward.

G. MOTION OF ELECTRONS IN PHASE SPACE

When considering how a beam of electrons behaves in phase space, one can think of the description as the superposition of the contributions of many individual electrons. With many electrons under study, however, one can now describe larger scale phenomena that are important to the operation of the FEL. For instance, in Figure (7), there is a distribution of electrons that have been displaced from resonance and have been injected with uniform distribution of ζ values across the light wavelength. In order for coherent radiation to take place, the electrons must get themselves into position so that they can radiate in phase. The “in phase” description is appropriate to our phase space discussion because if the electrons can achieve an orientation with respect to one another where they are “bunched” about some ζ , they will radiate in phase. Figure (7) shows a beam that has undergone bunching on its travel through the undulator. It is observed that the beam has bunched around $\zeta \approx \pi$, where they decrease in energy, and the optical field increases in strength. If the electron beam were allowed to continue bunching longer, the electrons would continue following their paths, eventually moving to a region in phase space ($\zeta \approx 0$) where they take energy from the light.

It should be noted that the phase space plots of a FEL will change over many passes as the optical field evolves. During start up when the optical field is small, the separatrix height, $2\sqrt{|a|}$ is small. If the electrons are injected off resonance, or have some spread in ν , then most of the electrons in the beam are in open orbits. In this configuration, it is difficult to achieve the significant extraction of energy from the electron beam. As the electrons give up a small amount of energy to the weak optical field, the field strength increases over many passes. This increasing field strength $|a|$ serves to expand the height of the separatrix. Once the separatrix is large enough to capture significant portions of the electron beam, extraction occurs on a larger scale. At some point, called “saturation”, the FEL reaches a steady state. In phase space, one would see that the electrons have continued their rotation and approximately as

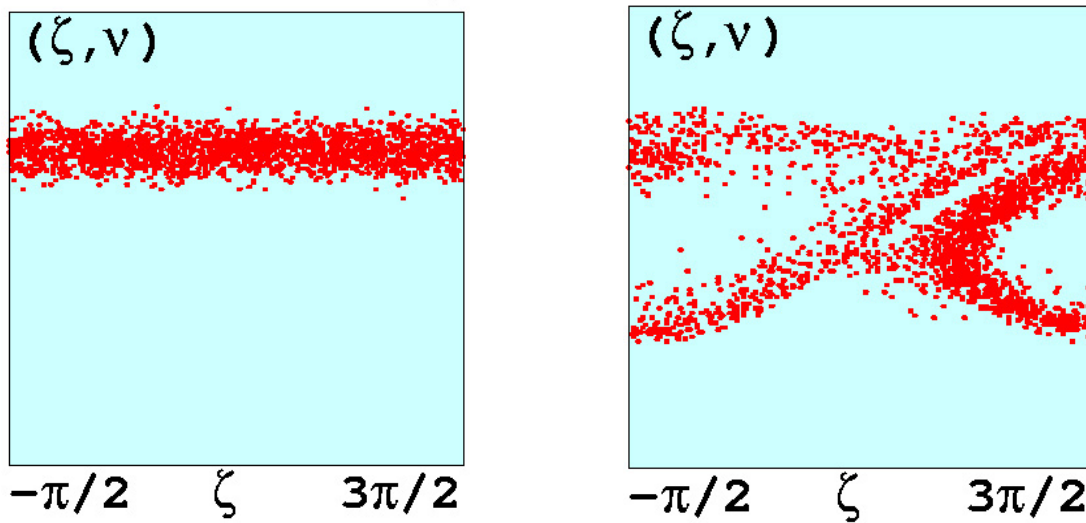


Figure 7. The figure to the left shows a beam of electrons injected into the undulator with a gaussian distribution of ν values and uniformly distributed in ζ . The figure to the right shows a beam of electrons at the end of the undulator having undergone bunching about the point $\zeta \approx \pi$.

many electrons have given up energy to the optical field (around $\zeta \approx \pi$) as have taken energy from the optical field (around $\zeta \approx 0$). Once the electrons begin to overbunch and take energy back from the optical fields, the FEL is in saturation and single-pass gain is reduced to match the single-pass resonator losses.

H. COHERENCE CHARACTERISTICS

One of the primary attributes that make lasers such useful tools is their ability to deliver light of high coherence and narrow spectral line widths. To this point, the previous sections have developed the theory necessary to show that a FEL will generate light through interaction with a highly relativistic electron beam. Initially, the light generated is neither coherent, nor of a narrow frequency. How do these qualities develop from a system that does not initially possess them?

When the FEL is started from noise, the electrons radiate non-coherently into the optical resonator of the oscillator. The light fields that initially develop contain many frequencies. As these fields build, they begin to interact with the electron

beam. As discussed previously, the electrons begin to bunch together slightly in phase space. As this bunching takes place, the electrons are able to radiate in phase with one another. The radiation is still in several frequencies, but when the gain curve of the FEL is taken into consideration, the wavelength corresponding to the highest point on the gain curve experiences the greatest growth. The coherence of the output light is a result of this wavelength's growth outstripping the other wavelengths over many passes as electrons radiate in the undulator.

THIS PAGE INTENTIONALLY LEFT BLANK

IV. OPTICAL THEORY

The physical development for how the electrons create light and interact with the light in order to generate laser output is complete. However, in order to accurately model the interaction of the light with the electrons, an understanding of how the light propagates after leaving the interaction region is useful. In addition, this same propagation knowledge serves to model how the laser light acts after it leaves the FEL and propagates to the target.

A. THE OPTICAL WAVE EQUATION

As light can be considered as a wave, it can be treated with the same methodologies that are applied to radar, acoustics, and other wave phenomena. In general, the wave evolution is determined by the following Equation (assuming the Coulomb gauge), where \mathbf{A} is the optical vector potential satisfying $\mathbf{E} = -(1/c)\partial\mathbf{A}/\partial t$ and $\mathbf{B} = \nabla \times \mathbf{A}$ and \mathbf{J}_\perp is the current flowing perpendicular to the direction of travel of the light field,

$$\left(\nabla^2 - \frac{1}{c^2} \frac{\partial^2}{\partial t^2} \right) \mathbf{A}(\mathbf{x}, t) = \mathbf{J}_\perp \frac{4\pi}{c} \quad . \quad (\text{IV.1})$$

Since this light wave is outside the interaction region, then there is no current present, thus

$$\mathbf{J}_\perp = 0 \quad .$$

The undulator from which this light created has a known magnetic field orientation, it is natural to assume that the polarization of the light outside the undulator is known. If we assume a helical undulator, then the light generated in the interaction between the light fields and the magnetic fields will have a helical polarization. The vector potential for a plane wave traveling in the z direction can be written as

$$\mathbf{A}(\mathbf{x}, t) = Re \left\{ \frac{\mathcal{E}(\mathbf{x}, t)}{k} e^{i(kz - \omega t)} \hat{\mathbf{e}} \right\} \quad . \quad (\text{IV.2})$$

The optical wavenumber, k , is equal to ω/c . The polarization vector, $\hat{\mathbf{e}}$, is $(-i, 1, 0)$. $\mathcal{E}(\mathbf{x}, t)$ is the complex optical field amplitude and phase and is equal to $\mathbf{E}(\mathbf{x}, t) e^{i\phi(\mathbf{x}, t)}$, where $\mathbf{E}(\mathbf{x}, t)$ is the amplitude and $\phi(\mathbf{x}, t)$ is the optical phase.

If ψ is defined as $kz - \omega t + \phi$, then a real-valued \mathbf{A} can be written

$$\mathbf{A}(\mathbf{x}, t) = \frac{E(\mathbf{x}, t)}{k} (\sin \psi, \cos \psi, 0) \quad .$$

Next, we assume that the optical amplitude and phase are both slowly varying in time and space, which can be used later to simplify the wave equation (dotted values are time derivatives and the primed values are spatial derivatives with respect to z),

$$\begin{aligned} \dot{E} &\ll \omega E \quad , \\ E' &\ll kE \quad , \\ \dot{\phi} &\ll \omega\phi \quad , \text{ and} \\ \phi' &\ll k\phi \quad . \end{aligned}$$

Substituting Equation (IV.2) into Equation (IV.1), and noting that $\hat{\mathbf{e}} \cdot \hat{\mathbf{e}}$ is equal to 2, we obtain a differential equation that describes both diffraction and propagation and has replaced the time and z dependence with lower order terms

$$\left[\frac{1}{2} \nabla_{\perp}^2 + ik \left(\frac{\partial}{\partial z} + \frac{1}{c} \frac{\partial}{\partial t} \right) \right] \mathcal{E} = 0 \quad . \quad (\text{IV.3})$$

In Equation (IV.3), the ∇_{\perp}^2 term is an operator consisting of the sum of the second order spatial derivatives in the perpendicular directions ($\hat{\mathbf{x}}$ and $\hat{\mathbf{y}}$). It is this part of Equation (IV.3) that describes diffraction. The second term of Equation (IV.3) describes the propagation of the wave along z .

To proceed with the development, let us introduce new time and propagation direction coordinates, $t \rightarrow \tau$ and $z \rightarrow \mathcal{Z}$, where

$$\begin{aligned} \tau &= \frac{ct}{R} \quad , \quad R \text{ is range of propagation, and} \\ \mathcal{Z} &= z - ct \quad . \end{aligned}$$

After we change the operator in Equation (IV.3), we obtain,

$$\left(\frac{i}{2}\nabla_{\perp}^2 - \frac{k}{R}\frac{\partial}{\partial\tau}\right)\boldsymbol{\mathcal{E}} = 0 \quad . \quad (\text{IV.4})$$

To continue the simplification process of Equation (IV.4), we find the scaling factors that are described in the operator. For now, assume that any changes in perpendicular spatial directions are equal ($\Delta x \approx \Delta y$), and attempt to find a scaling factor for the diffraction term. Moving the coefficients of the time dependent term to the diffraction term, we obtain

$$\left(\frac{iR}{2k}\nabla_{\perp}^2 - \frac{\partial}{\partial\tau}\right)\boldsymbol{\mathcal{E}} = 0 \quad .$$

Looking at the coefficient of the diffraction term and inserting Δx as a small change in the transverse direction,

$$\frac{R\lambda}{4\pi(\Delta x)^2} \quad ,$$

we can see that $\sqrt{R\lambda}$ is related to the wavefront size which is captured by Δx . If $\sqrt{R\lambda}$ is much less than the area of the optical mode, then the diffraction term is negligible. A plane wave has $\Delta x = \infty$, meaning the diffraction term $\rightarrow 0$. Thus, for an infinite plane wave, there is no diffraction. As expected, as the beam width decreases, the spreading of the beam due to diffraction increases. Thus $\sqrt{R\lambda}$ is a value that will be useful as a scaling factor.

The Rayleigh length, z_0 , is the characteristic distance over which the beam area doubles in size from its initial or waist area, defined by,

$$z_0\lambda = \pi w_0^2 \quad ,$$

where w_0 is the initial mode waist radius. If we let the Rayleigh length be the range over which we are interested, then the important radius is,

$$\begin{aligned} R\lambda = \pi w_0^2 &= \frac{2\pi R}{k} \quad , \\ w_0 &= \sqrt{\frac{2R}{k}} \quad . \end{aligned}$$

We now have the scale length in the transverse direction that we can use to scale the system of interest. The appropriate scale length in the propagation direction is the desired range. This results in $\tau = z/R$ where τ now varies from 0 to 1. We define a new set of dimensionless coordinates and substitute them into our wave equation operator, yielding

$$\begin{aligned} \tilde{x} &= x\sqrt{\frac{k}{2R}} \quad , \\ \tilde{y} &= y\sqrt{\frac{k}{2R}} \quad , \\ \frac{\partial^2}{\partial x^2} &= \frac{k}{2R} \frac{\partial^2}{\partial \tilde{x}^2} \quad \& \quad \frac{\partial^2}{\partial y^2} = \frac{k}{2R} \frac{\partial^2}{\partial \tilde{y}^2} \quad , \text{ and} \\ \left(\frac{-i}{4} \tilde{\nabla}_{\perp}^2 + \frac{\partial}{\partial \tau} \right) \mathcal{E} &= 0 \quad , \text{ where } \tilde{\nabla}_{\perp}^2 = \frac{\partial^2}{\partial \tilde{x}^2} + \frac{\partial^2}{\partial \tilde{y}^2} \quad . \end{aligned} \quad (\text{IV.5})$$

Equation (IV.5) can be recognized as the parabolic wave equation. In the wiggler of the FEL, there is also a source term due to the presence of a current.

Recalling the definition of \mathcal{E} in Equation (IV.2), we rename the complex optical field amplitude and phase as $a = |\mathcal{E}|e^{i\phi}$. Using this notation, and applying the operator defined in Equation (IV.5), we obtain the relation necessary to model the propagation of light in free space,

$$\frac{\partial a}{\partial \tau} = \frac{i}{4} \tilde{\nabla}_{\perp}^2 a \quad . \quad (\text{IV.6})$$

If we assume that the output beam of the FEL is Gaussian in shape, then it can be shown analytically that a solution to Equation (IV.6) is

$$a(r, \tau) = \frac{a_0}{w(\tau)} e^{[i\phi(\tau) - \frac{r^2}{w^2(\tau)z_0}]}$$

where $r^2 = x^2 + y^2$,

$$\begin{aligned} w(\tau) &= \sqrt{1 + \frac{(\tau - \tau_w)^2}{z_0^2}} \quad , \text{ and} \\ \phi(r, \tau) &= -\tan^{-1} \left(\frac{(\tau - \tau_w)}{z_0} \right) + \frac{r^2 (\tau - \tau_w)}{z_0^2 + (\tau - \tau_w)^2} \quad . \end{aligned}$$

The above equations provide the basis for creating a computer code to model the propagation of light (see Appendix A). With the appropriate operators introduced into the algorithm, many of the topics of concern for atmospheric propagation can be investigated.

B. PROPAGATION

Since the intent of a sea-based weapon system is to engage targets in and around the maritime environment, it makes sense to discuss the phenomena that affect the propagation of light through the atmosphere. The major atmospheric interactions considered here are absorption, scattering, turbulence, and thermal blooming.

1. Scattering

Atmospheric scattering is the second most important energy loss mechanism in the propagation of a laser beam. In this interaction with the atmosphere, the light field interacts with scattering centers in the atmosphere, such as water droplets and dust, and the energy is redistributed in directions that may not contribute to the intended use of the laser. There are three primary atmospheric scattering processes which are listed in Table (I).

Type of Scattering	Size of Scatterer
Rayleigh Scattering	Larger than electron but smaller than λ
Mie Scattering	Comparable in size to λ
Nonselective Scattering	Much larger than λ

Table I. Types of atmospheric scattering [9]

Rayleigh scattering is a process in which the incident electric field causes local charge separation by inducing a dipole in the scattering center, typically an individual molecule. This dipole oscillates with the same frequency of the incident light field.

An accelerating electric charge radiates, retransmitting the energy absorbed from the electric field. The radiation from Rayleigh scattering is emitted in all directions, causing a loss of energy in the light field as it propagates through the atmosphere. This type of scattering is highly wavelength dependent (proportional to λ^{-4}), and for wavelengths greater than 1 micron can usually be neglected [9].

Mie scattering takes place when the scattering centers are comparable to the size of the wavelength incident. These types of scattering centers are typically suspended aerosol particles and very small droplets of water. In Mie scattering, the same process of dipole formation takes place, however the spatial effects (nonuniform electric field) can no longer be ignored. The reradiation of incident energy, like Rayleigh scattering, is in all directions, however Mie scattering results in much more energy being radiated in the direction of incident light travel. As the size of the scattering center increases, the energy radiated by the scattering center becomes much more directional, as suggested in Figure (8)

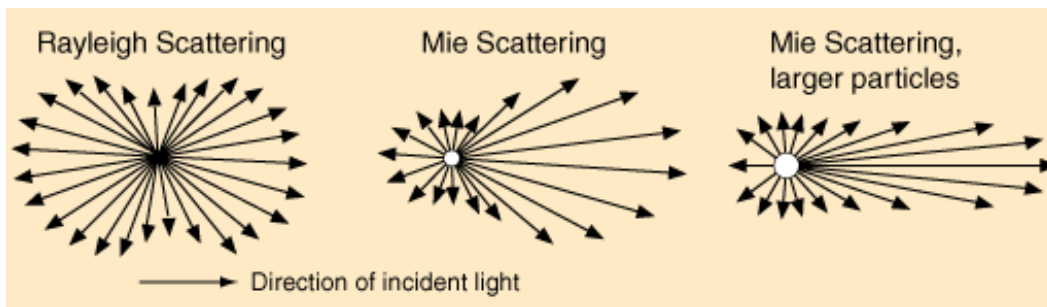


Figure 8. Rayleigh and Mie scattering radiation patterns [5]

Nonselective scattering is the mechanism that describes what happens to light incident or passing through atmospheric phenomena such as fog, haze, and clouds. As Table (I) describes, nonselective scattering occurs when the size of the scattering center is much larger than the incident wavelength of light. The term nonselective implies that this type of scattering is independent of the wavelength. Another mechanism that must remain in the forefront when dealing with this type of scattering is

that the scatterer size also allows for significant absorption in addition to the light being reradiated in undesired directions.

2. Absorption

Absorption is a process where energy is removed through interaction with materials which are suspended in or make up the medium in which the beam is propagating. This interaction, much like the interaction of electromagnetic radiation impinging upon some material, is described by an exponential decay governed by the absorption coefficient, α . The irradiance incident upon a target is described by the following, where I is the irradiance at some range, z , and I_0 is the initial irradiance

$$I(z) = I_0 e^{-\alpha z} \quad . \quad (\text{IV.7})$$

The absorption coefficient in the atmosphere is dependent upon the size of the suspended materials, the type of materials suspended, and the frequency of the light that is being considered. The primary atmospheric components that contribute to absorption are water (H_2O), carbon dioxide (CO_2), diatomic oxygen (O_2), and ozone (O_3). These molecules absorb the electromagnetic radiation of the propagating beam and convert it to molecular vibration and rotation [9].

In a practical system, there is no way to control the content of the atmosphere through which the beam is intended to propagate, therefore the best alternative is to choose a wavelength of light that is not greatly affected by absorption. The atmosphere is said to have “windows” of propagation where the absorption is minimized. Figure (9) presents a graph of the transmittance (the amount of energy allowed to pass through the atmosphere) as a function of wavelength.

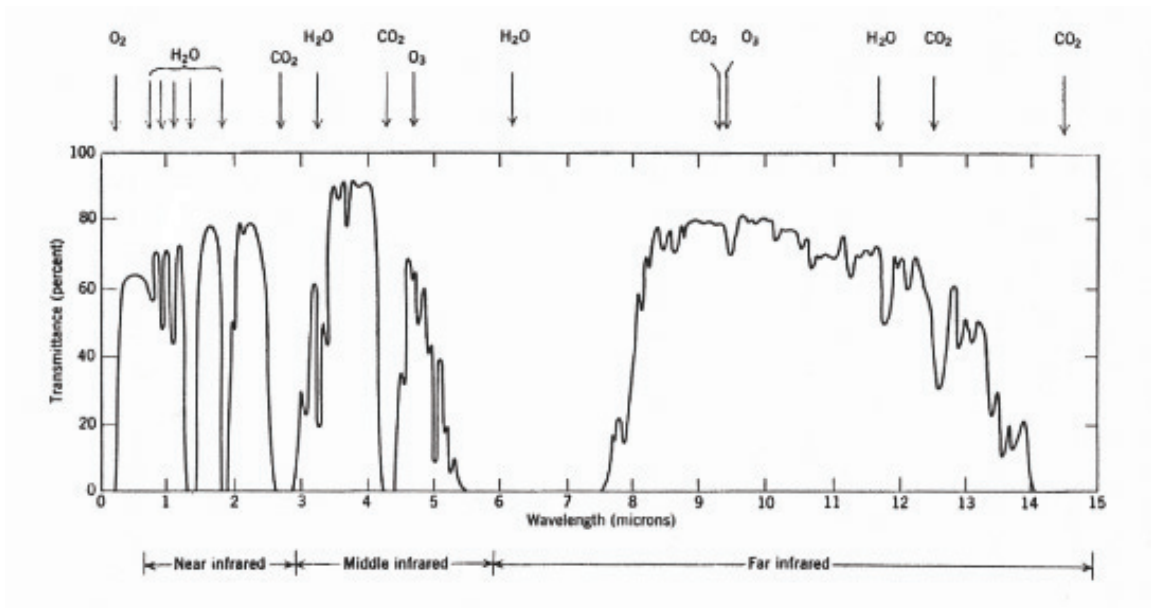


Figure 9. Atmospheric transmittance, which includes both absorption and scattering, over 1820-m horizontal path at sea level [6, p. 115]

3. Thermal Blooming

Thermal blooming is a defocusing effect where the energy in a laser beam spreads away from its center. Energy deposition in the transmission medium (air) is proportional to the local intensity of the beam. Absorption contributes to thermal blooming, but scattering does not. Since we assume a Gaussian beam intensity profile, the greatest intensity is initially in the center. As the air heats up, the local index of refraction decreases, allowing the light passing through that location to move faster than the light in the remainder of the beam [10]. The effect is a shift in the phase front of the beam that diffracts beam energy away from the beam axis.

Thermal blooming can be controlled in a variety of ways. Reducing the intensity of the beam will reduce blooming effects, as will spreading out the beam. Beam spreading can be accomplished by increasing the size of the beam at the director. In a weapons application, we want the greatest amount of fluence (Intensity per unit time) on target, so that a large beam at the director is focused at the target. As the beam focuses, the local intensity increases and the thermal blooming threshold can be exceeded again. If thermal blooming occurs near the target, it is of reduced consequence, because the beam does not have time to spread before hitting the target.

Cross wind clearing can also alleviate, though not eliminate, thermal blooming. The natural movement of air in the atmosphere, ie. wind, causes an exchange of air within the beam[10]. This moves the hottest portion of the beam away from the center, causing the wavefront to expand as before, but this time along a vector that tends to “bend” the beam into the wind. Significant to close-in engagements, the slewing of the director to keep the beam on target causes another source of apparent wind that increases cross wind clearing. During an engagement, a region along the propagation path experiences no apparent air motion, and this “stagnation zone” is typically where blooming will take place.

4. Turbulence

Turbulence has been extensively studied, especially in the field of astronomy where it is of major concern for ground based telescopes. It has also been extensively studied in the case of satellite communications. However in a weapons application, especially one where the platform and target are deep within the lower levels of the atmosphere, turbulence can be a more significant concern. In satellite or telescope applications, the light travels near vertically through the atmosphere and quickly leaves the thick, highly turbulent layers near the surface. Warfare applications tend to be near horizontal; even in vertical applications, they tend to be of short range (on the order of 10's of kilometers).

Turbulence is an atmospheric phenomena driven by temperature fluctuations in the atmosphere. As the land heats or cools due to the diurnal light cycle, heat is dissipated through convective motion of the air. Since light is traveling through the atmosphere and not through a vacuum, these temperature fluctuations will have an impact on the propagation of the light. As the local temperature changes, so does the local index of refraction. The scale size of these index of refraction regions is influenced by the scale size of the turbulence which created them. The Kolmogorov theory describes the atmosphere's dissipation method as the formation of eddies or "turbules" which transfer energy into smaller and smaller regions until viscous forces can dissipate the temperature differences. [7, p. 45]

Andrews and Phillips [7] have an excellent development of the statistics of turbulence that builds upon the more difficult papers of the Russians, Kolmogorov and Tatarski. Since we are not so much concerned with the internal dynamics of how turbulence occurs, but want to model the beam wander associated with turbulence, we find that the primary measure of turbulence strength is the index of refraction structure constant, C_n^2 . In descriptive terms, weak turbulence has a typical value of $C_n^2 = 10^{-17}m^{-2/3}$ and strong turbulence is typically on the order of $C_n^2 = 10^{-13}m^{-2/3}$ [7].

The structure constant has a strong altitude dependence and can be described by many models from an analytic form provided by Fried [11] to more complicated ones such as the Hufnagel-Valley model and the submarine laser communications day and night models. As altitude increases, turbulence strength (C_n^2) tends to decrease.

From a propagation standpoint, the primary effect of weak turbulence is to cause the beam to wander because the turbules are of the order of the beam size. In moderate turbulence, wander is suppressed, though still present, and the beam begins to broaden and scintillate. Scintillation is the “internal breaking up of the beam spot into smaller ‘hot spots’” [9].

C. COMPUTER MODELING

In order to gain an understanding of atmospheric propagation, computer simulations are used to model what a laser experiences in propagating through the atmosphere. With the exception of absorption, as is discussed first, phenomena can be modeled with phase shifts of the wavefront using “thin” phase screens. “Thin” means that the thickness of the phase screen is small compared to the propagation distance of the laser.

1. Scattering and Absorption

Absorption and scattering are both energy loss mechanisms. Examples of typical absorption and scattering profiles are shown in Figures (10) and (11). Most models show that the majority of the absorbing material is found in the lower portion of the atmosphere. Through this layer, α , the extinction coefficient, is fairly constant. Above this layer, α drops quickly to smaller values. We can determine the total extinction by integrating the extinction coefficient along the slant path from the transmitter to the target. From this we can determine the intensity that reaches the target,

$$I_{\text{target}} = I_0 \int_{\text{transmitter}}^{\text{target}} e^{-\alpha(x)} dz \quad , \quad (\text{IV.8})$$

where I_0 is the initial intensity at the transmitter, x is the altitude, and z is the slant range. As an example calculation, representative of the engagement scenarios in Chapter (VI), the transmittance (I_{target}/I_0) is 0.67 for 30 km propagation distance looking in the zenith direction and 0.33 for 30 km propagation horizontally through the Summer Maritime 14.8 km atmosphere at $1.045 \mu\text{m}$ wavelength.

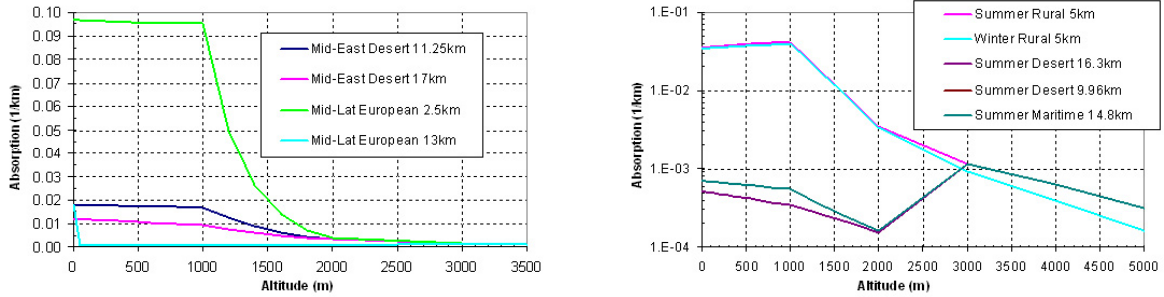


Figure 10. Various atmospheric absorption profiles [12]

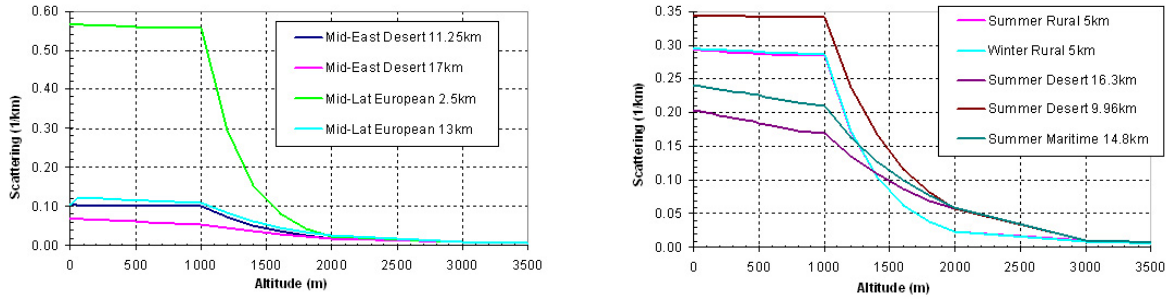


Figure 11. Various atmospheric scattering profiles [12]

2. Thermal Blooming

Thermal blooming is a redistribution of optical energy due to absorption and resulting local heating in the atmosphere. The propagating beam changes the index of refraction and causes a lens effect. Since the energy absorbed as heat is proportional to the energy incident, we can model the thermal blooming effect with an energy-weighted lens, making the assumption that energy loss to absorption causing the blooming can be ignored until the target is reached.

The energy at each point (\tilde{x}, \tilde{y}) on the wavefront can be determined by squaring the magnitude of the optical field, $a(\tilde{x}, \tilde{y})$. The strength of the blooming can be scaled using a scaling factor, ϕ_b . Thus a lens is created, introducing a phase shift (Φ) across the wavefront simulating thermal blooming,

$$\Phi(\tilde{x}, \tilde{y}) = [a(\tilde{x}, \tilde{y})^* a(\tilde{x}, \tilde{y})] \cdot \phi_b \quad . \quad (\text{IV.9})$$

To demonstrate the effects of thermal blooming, various values for ϕ_b are applied to a weaponized Gaussian beam. This beam has a dimensionless Rayleigh length $z_0 = 0.3$ and the beam waist is located at the target, $\tau = 1$. Figure (12) demonstrates a beam propagating in the absence of thermal blooming. Figure (13) shows a beam with “mild” blooming, $\phi_b = 6.0$, and mid-point stagnation, $\tau_b = 0.5$. Figure (14) shows a beam experiencing “moderate” blooming with $\phi_b = 6.0$ and a stagnation point near the target $\tau_b = 0.8$. The stagnation zone is where blooming takes place. It is the region in the propagation path that experiences zero relative motion when wind and the engagement dynamics are taken into consideration. Of note in Figures (13) and (14), is that due to focusing of the beam, the blooming effect increases as τ_b moves closer to the target. However, when τ_b gets close enough to the target, the beam does not have time to diffract the energy outward and the beam is essentially unperturbed.

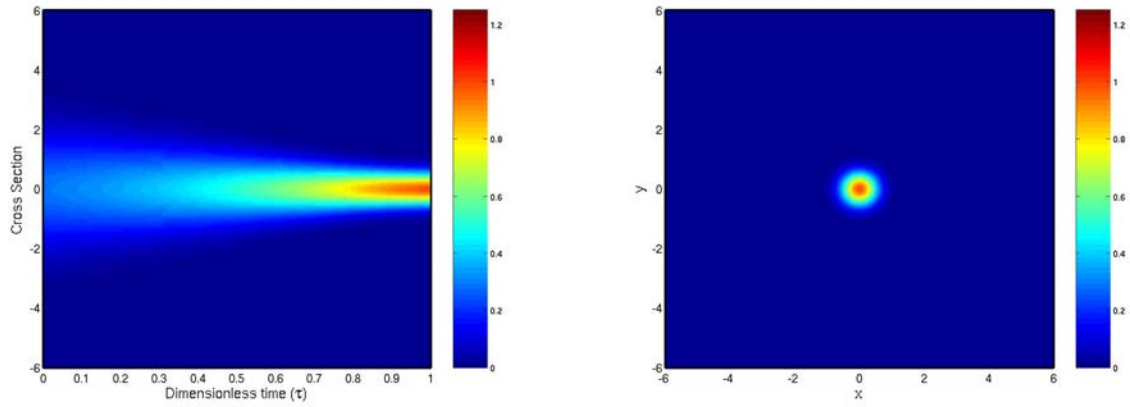


Figure 12. The picture to the left is a top down view of a propagating beam. The picture to the right is a cross section of the beam at the target. No blooming ($\phi_b = 0$) is present in this case.

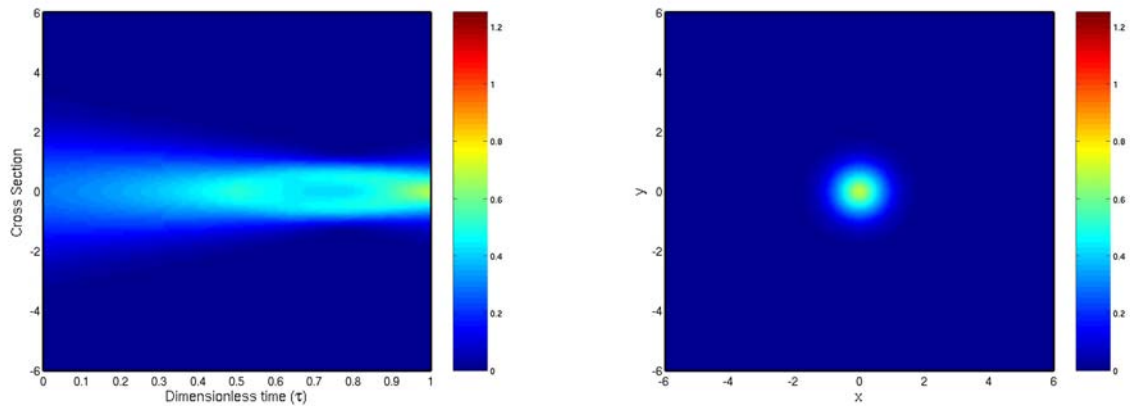


Figure 13. A propagating beam experiencing mild thermal blooming at stagnation point $\tau_b = 0.5$ with strength $\phi_b = 0.6$. The picture to the right is a cross section of the beam at the target.

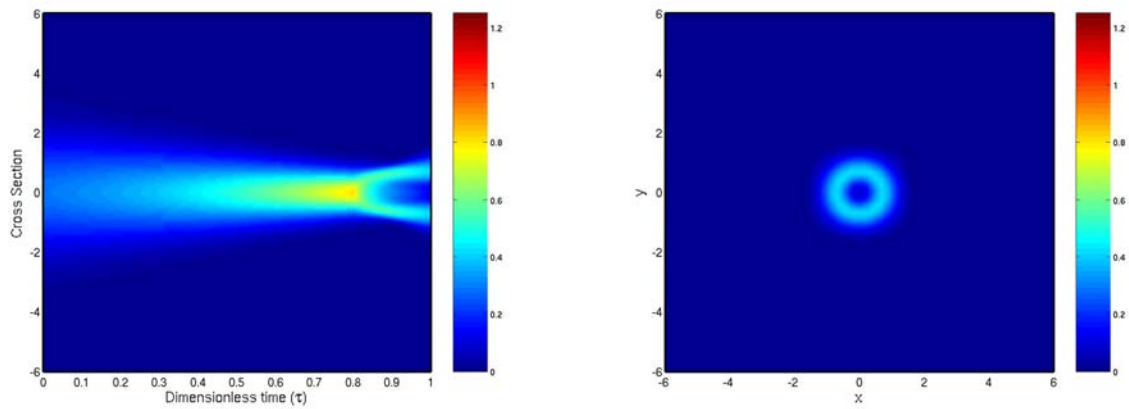


Figure 14. A propagating beam experiencing moderate thermal blooming at stagnation point $\tau_b = 0.8$ with strength $\phi_b = 0.6$. The picture to the right is a cross section of the beam at the target.

3. Turbulence

The modeling of turbulence is much more complicated than previously discussed phenomena. The primary methodology is to model the extended turbulent atmosphere, Figure (15), as a series of phase screens of finite extent, see Figure (16), that perturb the propagating beam in such a way that it models the effects of the extended medium.

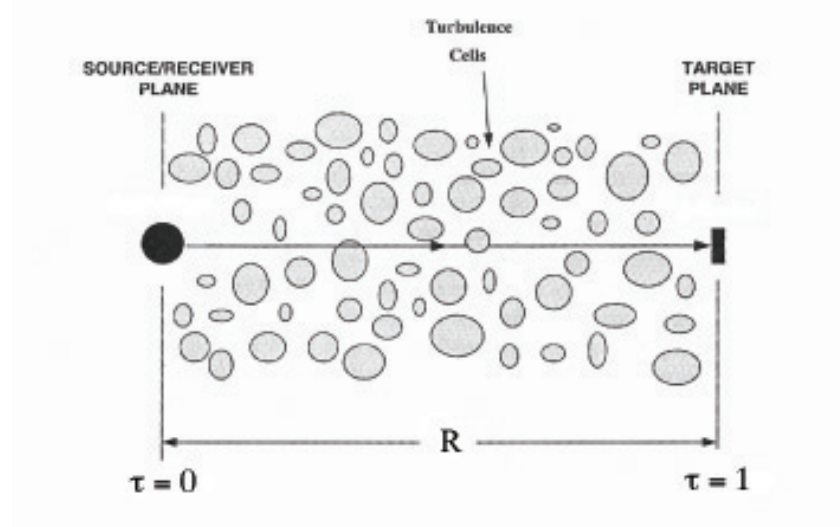


Figure 15. An extended turbulent medium [7]

There are many different perturbations that turbulence imparts to the propagating beam. When the turbule sizes are on the same order of the beam diameter, the beam deflects from its path. This results in the beam centroid wandering around the unaffected beam centroid location. If the turbule sizes are smaller than the beam diameter, the beam is internally broken up. This leads to scintillation, locations of random levels of intensity, and beam broadening, the widening of the beam over that of a diffraction limited beam. Figure (17) depicts both types of turbules and their effects on a propagating beam.

To represent the turbulence encountered by a beam as it propagates, we insert regions of turbulence in the form of phase screens which impart localized phase

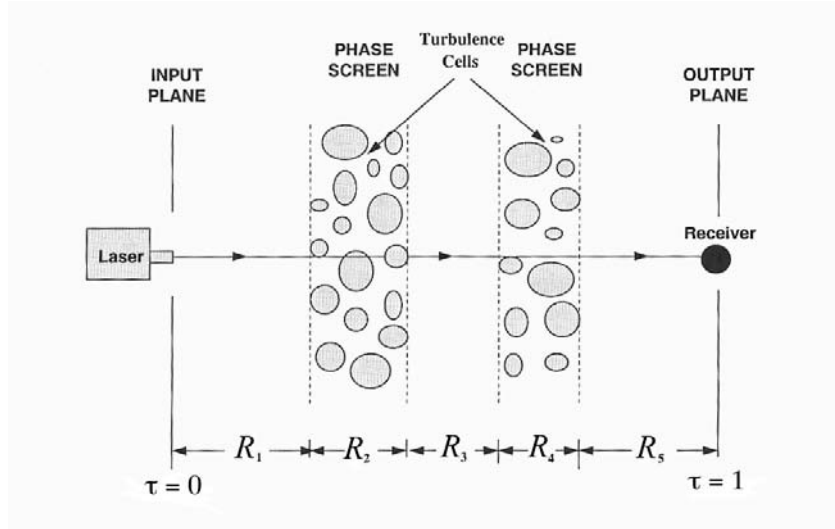


Figure 16. Multiple phase screens used to simulate an extended turbulent medium [7]

shifts on the beam. Referring to Figure (16), we consider a thickness of a region of turbulence that is much less than the propagation distance and represent it as a phase screen. The phase screen is “thin” and treated as an instantaneous phase shift, ie. the phase screen has a thickness of zero but represents the phase shifts over a distance. To generate the phase screens, we apply a general Fourier approach, attempting to capture the phase shift topography that would be encountered in the extended medium.

Starting from the one dimensional power spectral density for refractive index fluctuations of the Kolmogorov distribution [7],

$$\Phi_n = 0.022 C_n^2 k^{-\frac{5}{3}}, \text{ where } k \text{ is the scalar wavenumber,} \quad (\text{IV.10})$$

we can begin to develop a distribution of wavenumbers that can be used to develop a turbulent phase screen.

We assume that the propagation path will be horizontal, which removes the altitude dependence of C_n^2 . Next, we assume that C_n^2 remains constant along the

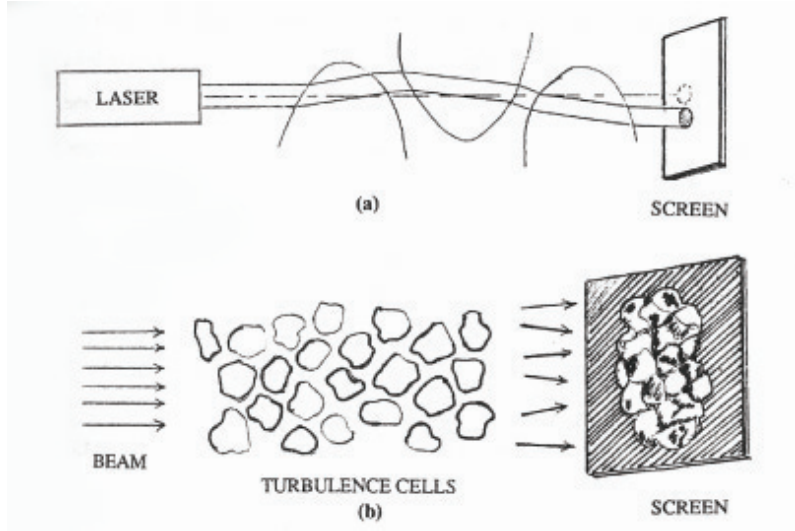


Figure 17. The upper picture depicts a wandering beam due to “large” turbules, while the lower picture depicts beam broadening and scintillation due to “small scale” turbules [7]

propagation path. We can then say that the optical field has a probability that some wavenumber, k , in the distribution is

$$P(k) = \sqrt{\Phi_n} \propto k^{-\frac{5}{6}} \quad . \quad (\text{IV.11})$$

To convert a uniformly distributed random number r into the desired distribution defined by Equation (IV.11), we use the cumulative distribution method. The following integral, shows that $k^{-5/6} \propto r$,

$$\int_0^k k'^{-\frac{5}{6}} dk' \propto k^{-\frac{1}{6}} \propto r \quad .$$

Continuing in this manner, we have

$$\begin{aligned} r &\propto k^{-\frac{1}{6}} \quad , \\ k &\propto r^6 \quad , \text{ leading to the general result} \\ k &= k_0 r^6 + b \quad . \end{aligned} \quad (\text{IV.12})$$

In Equation (IV.12), k_0 and b are arbitrary constants that can be used to determine the physical distribution. Essentially, they are fitting parameters that allow the user to match the resulting distribution of wavenumbers to the probability curve. Figure (18) shows the power spectral density as a function of wavenumber.

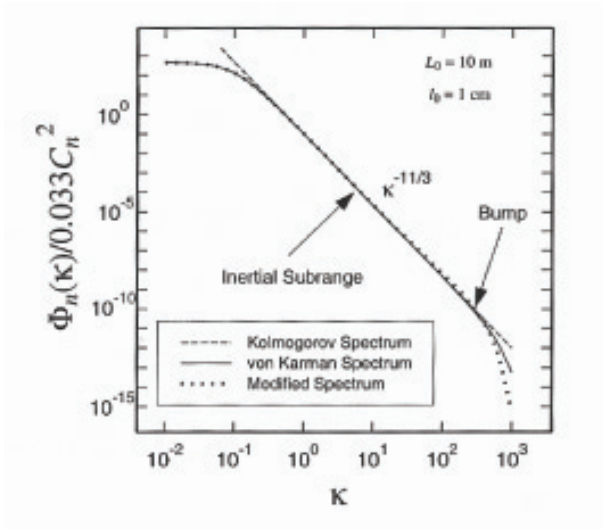


Figure 18. Kolmogorov power spectral density [7, p. 55]

The process of generating turbulent phase screens is to first choose a reasonable number of components to include. Then, using the distribution of Equation (IV.12), wavenumbers are chosen. Each wavenumber can be thought of as a single pane of glass into which a sine wave is ground, with a wavelength corresponding to the chosen wavenumber. This sine wave is given a random rotation about the z axis (from a uniform distribution) and stacked as in Figure (19). The process continues until the desired number of wavenumbers are chosen. Since this is a computer simulation, the “panes of glass” that have been stacked have zero thickness, and their amplitude corresponds to the amount of phase shift that will be applied at each point on the screen.

We assume that one desires to use multiple (N_p) phase screens along the propagation path, the phase effect of each screen must be scaled by $1/N_p$ [7]. Also,

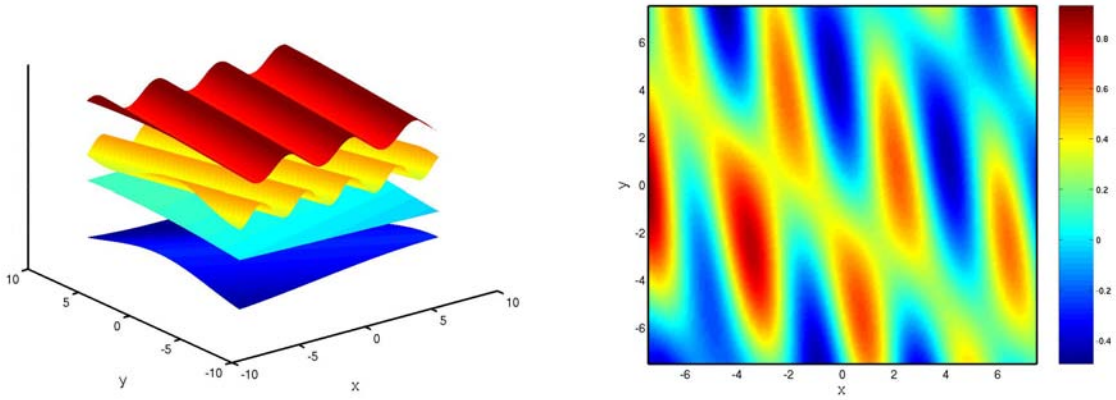


Figure 19. Individual phase sheets are generated (left), then stacked to create the final phase screen (right)

each screen is scaled by $1/M_p$, where M_p is the number of components that are used to make up each screen at each location. Figure (20) demonstrates how the constant k_0 can be used to determine the size of the characteristic turbule regions in the phase screens. As can be seen in Figure (20), as k_0 increases, the size of the turbule regions decreases. A beam passing through a larger k_0 screen experiences beam spread and scintillation while one passing through smaller k_0 experiences beam wander. Figures (21) and (22) demonstrate two beams propagated through turbulence, with Figure (21) demonstrating “large” turbules leading to wander and Figure (22) demonstrating “small” turbules leading to beam spread and scintillation. Both figures are plotted using the same random number seed, so turbule scaling is equivalent to that seen in Figure (20).

The wander of the optical beam can also be tied to a turbulence value based upon the statistics gathered by passing multiple beams through a turbulence phase screen setup. We choose some number of components to be used in phase screen generation, the number of screens to place in the propagation path, and a strength multiplier ϕ_t . At the target screen, the centroid of the beam can be determined using an intensity weighted position average. In large scale turbulence, this centroid will

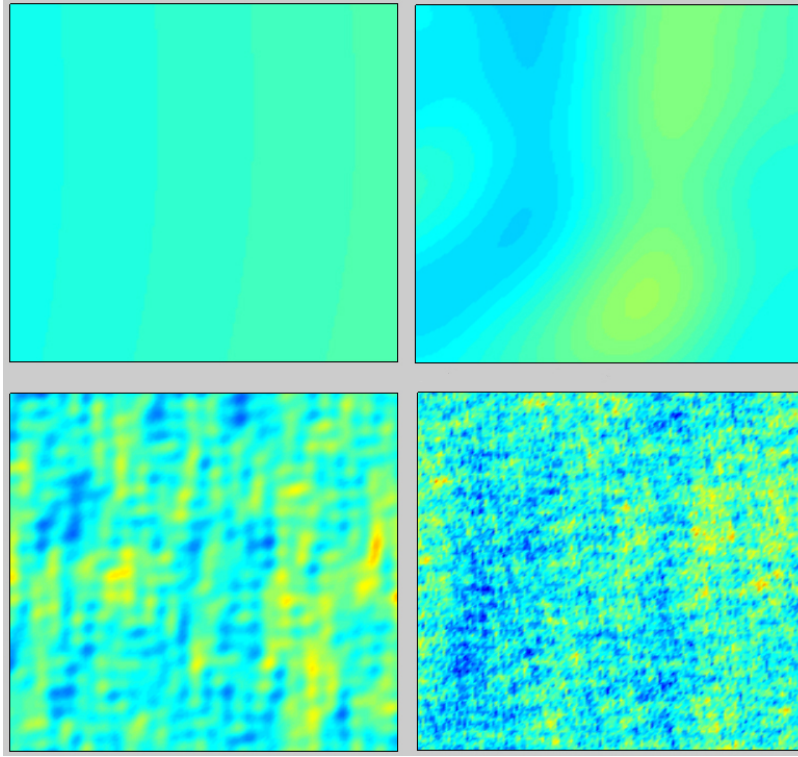


Figure 20. Each panel represents a phase screen composed of 100 components, a turbulence scaling factor (ϕ_t) of 10, and the color scale runs from $-\pi$ (blue) to π (red) and zero is green. From top left to bottom right, each panel represents a scale determined by k_0 of 0.01, 0.05, 0.1 and 0.5 respectively.

wander according to Equation (IV.13), where w_0 is the beam radius at the transmitter, R is the propagation distance, and σ^2 is variance of the final centroid position in the transverse direction at the target,

$$\sigma^2 = 1.44C_n^2 R^3 w_0^{-\frac{1}{3}} \quad [7, \text{p. 147}] \quad . \quad (\text{IV.13})$$

Equation (IV.13) can be rewritten in terms of the propagating wavelength for a Gaussian mode. Starting from the definition of the Rayleigh length and solving for

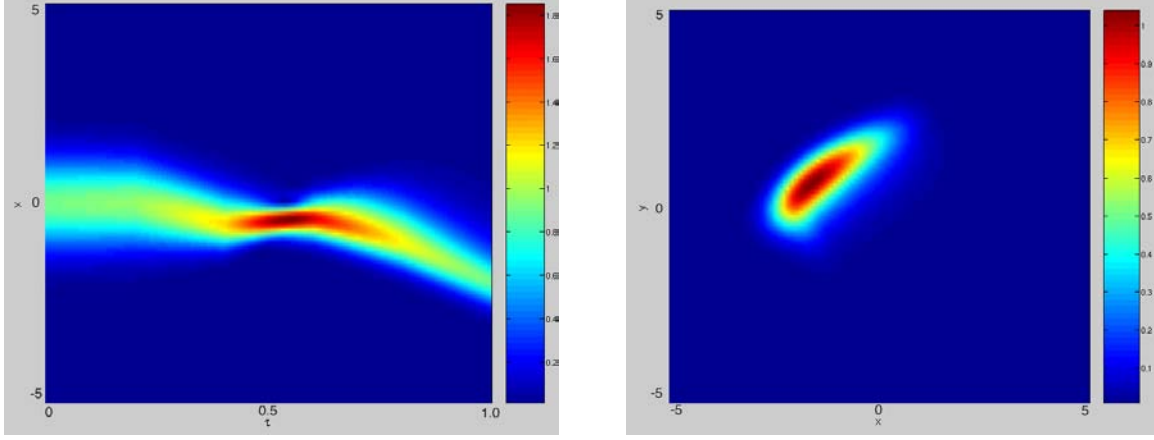


Figure 21. Beam wander due to large scale (small k_0) turbules. Pertinent values: $k_0 = 0.01$, $\phi_t = 500$, Number of Screens = 4, Components per screen = 20, $z_0 = 1.0$, $\tau_{\text{waist}} = 0.5$.

w_0 ,

$$\begin{aligned} z_0 &= \frac{\pi w_0^2}{\lambda} , \\ w_0 &= \sqrt{\frac{z_0 \lambda}{\pi}} . \end{aligned} \quad (\text{IV.14})$$

Substituting Equation (IV.14) into Equation (IV.13), we obtain a description of the variance of the beam wander as a function of the wavelength used, the range of propagation, and the Rayleigh length of the beam,

$$\begin{aligned} \sigma^2 &= 1.44 C_n^2 R^3 \left(\frac{z_0 \lambda}{\pi} \right)^{-\frac{1}{6}} , \\ &= 1.44 \pi^{\frac{1}{6}} C_n^2 \left(R^3 z_0^{-\frac{1}{6}} \right) \lambda^{-\frac{1}{6}} , \\ &= 1.74 C_n^2 \left(R^3 z_0^{-\frac{1}{6}} \right) \lambda^{-\frac{1}{6}} . \end{aligned} \quad (\text{IV.15})$$

A number of beams are propagated through random phase screens along the turbulent path using the same parameters (ϕ_t , number of screens, and number of screen components), a distribution of beam centroids can be found. Since this turbulence process is isotropic, the directions $\hat{\mathbf{x}}$ and $\hat{\mathbf{y}}$ are arbitrary, implying that if we measure the variance of the displacement in x , the overall displacement variance

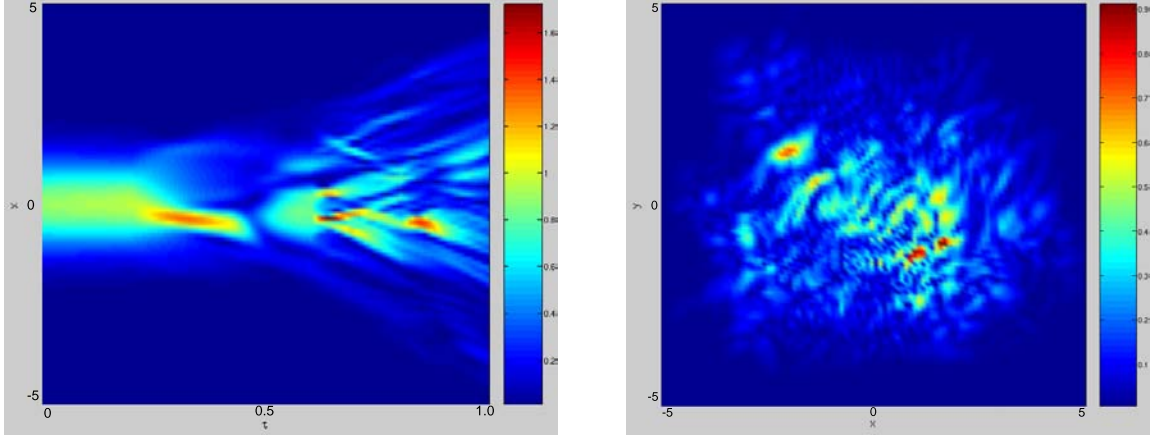


Figure 22. Beam spread due to small scale large k_0 turbules. Pertinent values: $k_0 = 0.1$, $\phi_t = 100$, Number of Screens = 4, Components per screen = 20, $z_0 = 1.0$, $\tau_{\text{waist}} = 0.5$.

is twice the variance in x as there is no preferred direction. Over a definite region, the behavior of ϕ_t is linear with respect to the C_n^2 that can be determined from the wander variance and Equation (IV.15). However, at some point, the effect of ϕ_t saturates, and begins to cause scintillation and beam spreading instead of wander. This effect is demonstrated in Figure (23). Essentially, the effect of increasing ϕ_t is to “stretch” the phase screen. Local phase change values near zero tend to remain near zero, however greater phase changes are increased much more than the near zero values. The result is that the regions of common phase become smaller, essentially making the same change to the phase screen that increasing k_0 does, though with much sharper boundaries between regions. The effect of increasing ϕ_t is incremental when compared to the effect of changing k_0 .

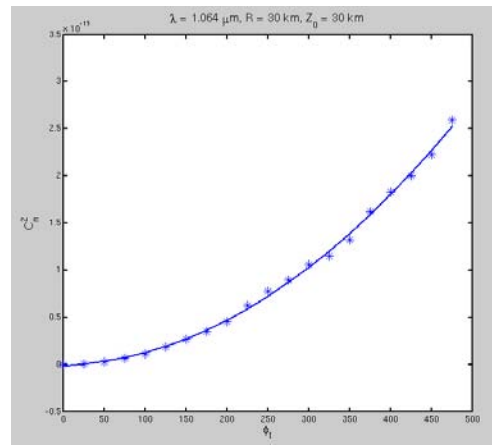
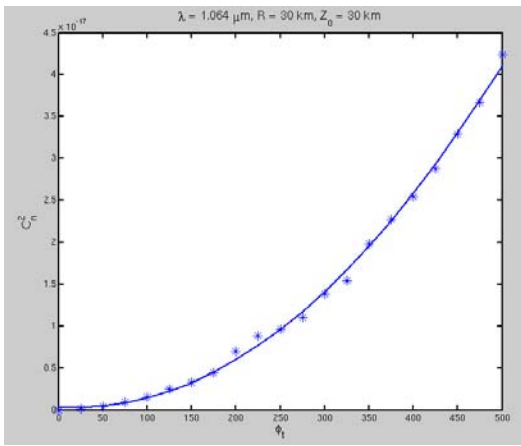


Figure 23. C_n^2 as determined by beam wander over a propagation distance of 30,000m. Left plot shows C_n^2 for a beam with k_0 of 0.01. Right plot shows C_n^2 for a beam with k_0 of 0.1.

V. SHORT RAYLEIGH LENGTH SYSTEMS

In order to weaponize a FEL, the system must be designed to fit within the constraints of current naval ship construction. A high output laser system must transport the high intensity laser light from the FEL to a beam director and out to the target without damaging the optics. Resonator optics, where the light intensities will be greatest, are the greatest concern.

Doubt has been expressed that the simulations using short Rayleigh length designs to minimize incident irradiance on the mirrors do not properly model the weak optical field gain. However, simulations based upon current system parameters indicate that there is no penalty, no loss in gain, when moving to shorter Rayleigh length systems, even though wide-spread, simple theory seems to contradict this.

A. SIZE CONSTRAINTS

The drive to put a large complicated system such as a FEL aboard a ship faces many difficult issues. Ships (even aircraft carriers) do not have unlimited available space. Attempting to put these systems aboard smaller vessels, such as destroyers, cruisers, and amphibious ships, will face even more stringent space, weight, and power constraints.

The FEL is not just composed of the accelerator, wiggler, and optics. In addition there are many pieces of auxiliary equipment, such as cryogenic cooling, RF klystrons, and the cooling systems for deposited heat in the optical train and in the beam dump. All of these systems have power requirements that are not constant loads. The transient nature of the power drawn by the system means that the power system of the ship in which it is installed will be highly taxed intermittently, indicating a need for some sort of power conditioning and storage. This implies even more volume and weight that must be taken up on the receiving ship.

The primary components of the system present their own issues. Linear ac-

celerators tend to be fairly large devices, especially when designed to reach shorter optical wavelengths, which require more beam energy. However, designs for moderately high energy electron beam accelerators (>100 MeV) have been proposed that have a foot print of less than 15 m in length. If these designs prove successful, then the limiting component for making the machine compact becomes the optical resonator. The resonator length cannot be arbitrarily short, but could be reduced by using a short Rayleigh length, allowing the resonator mirrors to be brought closer together. This has implications in other design considerations that will be discussed later.

B. OPTICAL DAMAGE

As the output power is raised to megawatt level, the optical power inside the resonator increases greatly. Looking at designs that have been proposed, optical outcoupling levels have been quoted as high as 50%. If outcoupling is 50%, then the optical resonator components must be capable of handling several megawatts on their surfaces. At these power levels, damage to the optics becomes a very real possibility and will affect the system's ability to continue lasing.

If one considers an average irradiance damage threshold of 100 kW/cm^2 [13, p. 51], this requires a circular area of 20 cm^2 ($w = 2.5 \text{ cm}$ radius) to 60 cm^2 ($w = 4.4 \text{ cm}$ radius) for output powers of 1 MW and 3 MW, respectively. We can determine the length of the resonator required using a "typical" dimensionless Rayleigh length ($z_0 = \pi w_0^2/L\lambda$) of 0.5, where L is assumed to be 1 m and the optical wavelength is $\lambda = 1.06 \text{ }\mu\text{m}$,

$$z = z_0 \left[\left(\frac{w}{w_0} \right)^2 - 1 \right]^{\frac{1}{2}}, \quad (\text{V.1})$$

where w_0 is the radius of the optical mode waist. Using Equation (V.1), we find that to allow the beam to diffract to the required areas, the resonator must be at least 60 m and 100 m for 1 MW and 3 MW machines, respectively. These lengths are on the order of half the length of an Arleigh Burke destroyer and are far too great to be considered seriously in a shipboard installation. Using a short Rayleigh length

resonator would allow the optical beam to diffract much more rapidly to the required area in a shorter distance. If, for example, z_0 were taken as a moderate level of 0.2, the lengths could be reduced to 40 m and 70 m, which are still too long to be seriously considered. If a fairly aggressive z_0 of 0.05 is considered, then the 1 MW system will fit within a 20 m footprint and the 3 MW resonator is twice that. This indicates that if a FEL is to be seriously considered as a HEL weapon system, the short Rayleigh length system, with quite small z_0 values must be explored.

Obviously, the large amount of outcoupling from the resonator assists the mirrors in surviving the damage of the high irradiance. However, this presents a conundrum to the FEL designer in that for a system to successfully outcouple 50% of the light, it must also create more light than is lost through the outcoupler for the system to reach the saturation power necessary for the desired output power. The wide-spread consensus in the FEL community is that there is not enough gain, which describes a system's ability to increase its power, in short Rayleigh length regimes. However, this belief is based upon theoretical development that applies only in the low current regime.

C. GAIN THEORY

Gain is the measure of a system's ability to amplify some input. In the case of a FEL, gain is a measure of the system's ability to increase the optical power. As each electron bunch passes through the undulator, energy is exchanged between the electrons and the electric field of the laser light. In a properly designed FEL, more energy is given to the laser fields by the electron beam than is taken by it. But gain must also take into account losses by other mechanisms, most importantly outcoupling.

We begin with how the gain develops as electrons progress through the linear undulator. In the limit of low gain, ($j < 1$), the optical gain $G = (P(\tau) - P_0) / P_0$ where $P(\tau)$ is the growing optical power and P_0 is the initial optical power, along

the undulator is given by

$$G(\tau) = j\bar{F} \left[\frac{2 - 2\cos(\nu_0\tau) - \nu_0\tau \sin(\nu_0\tau)}{\nu_0^3} \right] , \quad (\text{V.2})$$

where τ is the dimensionless time ($\tau = 0 \rightarrow 1$ along the undulator), ν_0 is the initial phase velocity, \bar{F} is the filling factor, and j is the dimensionless current density. The filling factor is a ratio of the cross sectional area of the electron beam to the optical beam. It is given by

$$\bar{F} = \frac{r_b^2 \pi}{L\lambda \left(z_0 + \frac{1}{12z_0} \right)} , \quad (\text{V.3})$$

where r_b is the waist radius of the electron beam and λ is the wavelength of light in the resonator [14]. The current density j is defined

$$j = \frac{8N [e\pi K (J_0(\xi) - J_1(\xi)) L]^2 n_e}{\gamma^3 mc^2} ,$$

where $\xi = K^2/2(1 + K^2)$, J_0 and J_1 are Bessel functions of the first kind, N is the number of undulator periods, L is the length of the undulator, and n_e is the number density of electrons [14].

The maximum overall gain of a FEL at $\tau = 1$ can be shown to be approximately

$$G \approx 0.135j\bar{F} , \quad (\text{V.4})$$

for $\nu_0 = 2.6$. As can be seen from Equation (V.3), as the Rayleigh length decreases to zero, the denominator becomes large and \bar{F} goes to zero, implying gain goes to zero as well. As z_0 increases, the optical mode waist becomes large compared to the electron beam so that $\bar{F} \rightarrow 0$, and $G \rightarrow 0$. What is not taken into account in Equation (V.4) is the interaction between the light and the electron beam. As the Rayleigh length decreases, the volume that it carves out at the ends of the undulator increases to the point where the volume of the electron beam is small in comparison, so $\bar{F} \rightarrow 0$ and $G \rightarrow 0$. The optimum \bar{F} is at $z_0 = 1/\sqrt{12}$. However, as z_0 decreases, the intensity of the light fields in the mode waist increase. This is not accounted for in the simple derivation of gain in Equation (V.4), and is numerically explored here. In the small

j regime, it makes sense that the FEL would experience very small gain, as there are few electrons with which the light can interact. When j increases beyond the low current limit, simulation results indicate more coupling allows for greater interaction in the waist area, generating sufficient gain for the FEL.

Using a FEL simulation [14], a short z_0 oscillator FEL can be studied over a range of currents and Rayleigh lengths. To benchmark the code, a range of currents were studied first at z_0 values comparable to machines that currently exist, $z_0 \approx 0.5$. The results show that the code agrees with the experimentally determined gain very well. When the low current regime is explored into the shorter z_0 regime, the resulting gain data displays the expected curve predicted by Equation (V.4). The surprising result occurs when, at these shorter Rayleigh lengths, a larger current, $j > 3$, is used. What we find is that the gain curve no longer drops to zero as quickly, but remains at acceptable gain levels to shorter and shorter z_0 as the current is increased. Figure (24) shows the results from many simulations.

The important concept that Figure (24) presents is that a short Rayleigh length FEL should have plenty of gain so long as the low current regime is avoided. But more importantly, the gains where the deviation from simple theory occur is very small, $G \approx 0.005j$ for $j \approx 5$, or only $G \approx 0.025 \approx 2.5\%$ gain. Nearly all FELs have gains greater than just a few percent so that nearly all FELs do not follow the simple theory.

In the case of a weaponized system, where the peak current is expected to be on the order of 1 kA, the dimensionless current will be well above 1, $j \approx 100$. For FEL designers attempting to decrease the size of their machines, this means that the short Rayleigh system is a viable option. Regardless of its impact on the weapon development considerations, these simulation results have pointed out a serious oversight in FEL theory. There is currently no theory to describe how the Rayleigh length affects gain when not in an extremely low current regime. In terms of experimentation, building a short Rayleigh length version of an existing machine would enable

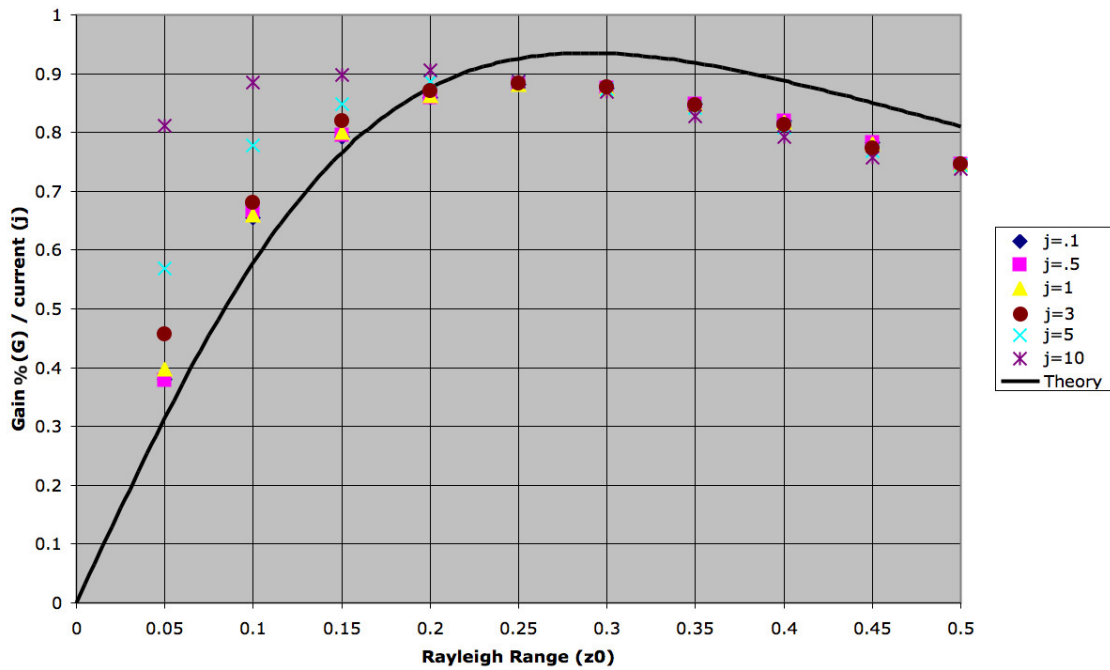


Figure 24. Gain curves for various Rayleigh lengths and dimensionless current values. Gain values have been normalized with respect to the current.

validation the simulation results even with a moderate decrease in z_0 . Jefferson Labs have performed some preliminary experiments with down to a z_0 of approximately 0.2 and seen higher gain than predicted by the simple theory [15]. Obviously, these results are encouraging and warrant continued study.

VI. THEATER BALLISTIC MISSILE DEFENSE

Theater ballistic missile defense (TBMD) becomes more important as the proliferation of theater ballistic missiles (TBM) continues. The TBM is more akin to the artillery shell than to the cruise missile, in that it is accelerated to its final velocity by a rocket motor and then falls ballistically to its intended target. The long range associated with a ballistic missile is due to the fact that most of its trajectory is above the drag effects of the atmosphere. In fact, intercontinental ballistic missiles can reach apogee heights of more than 1000 miles [16].

The U.S. Navy continues to move from a “blue water”, open ocean focused strategy to a littoral one. In the 20th century, battleships and aircraft carriers were the only ships to be considered “capital” ships. In today’s Navy, even a destroyer costs close to a billion dollars, and every ship on the U.S. naval register is a capital ship. As the operational focus moves closer to land and the abilities of other nations to develop weapons that have the range and accuracy to strike an Expeditionary Strike Group (ESG) or Carrier Strike Group (CSG) increases, naval forces need to develop an ability to counter this threat to their forces afloat and the supported landing forces ashore.

High energy lasers are currently being considered for use aboard ships as a self-defense weapon against the cruise missile threat. It is possible that this same laser can be used in a self-defense role against a TBM with an impact point close to an ESG or CSG. Based upon current open-source information regarding the sensor networks available to the Navy, an analysis of TBM defense scenarios can be conducted.

A. CURRENT STATUS

Various weapon systems and sensor systems have been developed to provide warning and counter-battery for ground and naval forces in support of theater oper-

ations. Currently, all fielded systems for area defense are based upon kinetic energy kills, whether by “skin-to-skin” direct hits or by showering the intercept area with small, dense rods. However, the Army and Air Force are developing directed energy weapons that can be used against TBMs.

1. Sensor Networks

The first part of any engagement is detection of the threat. Throughout the flight of the TBM, many types of sensors will be used to detect, identify, and track it. Launches are typically detected by their infrared signature, track data is developed from radar information, and identification can be made by infrared and other optical systems.

In the case of TBMs, there are many opportunities in which to acquire the TBM. Upon launch, all TBMs ride a plume of hot gases that are expelled from their rocket motors. Space-based sensors have been in place for years to detect these plumes. The Defense Support Program (DSP) satellites currently provide early warning coverage and initial tracking information [17]. The Space Tracking and Surveillance System (STSS) is scheduled to replace DSP in the 2006-2007 time frame and will provide greater ability to discriminate between TBMs and decoys, as well as better track data [17]. Once the TBM is well into flight, ground based radars can assist in developing track information.

Various radars are used to provide tracking coverage, including the Early Warning Radars in Alaska, California, and overseas, the Sea-Based X-Band Radar which can be towed to various locations, the SPY-1 radar found aboard Aegis cruisers and destroyers, and integral sensors to various weapon systems [17]. Once track data is accurate enough to generate a fire control solution, a weapon is paired and launched. These radars are then essential to make the kill/no-kill determination.

2. Weapons

Currently there are no high energy laser (HEL) weapons being used for TBMD. All weapons that are available for use in TBM engagements are kinetic kill weapons. Kinetic kill weapons depend on the collision between some type of kill vehicle or dispersed fragments from the anti-TBM weapon and the TBM.

Since the TBM is typically launched from some point well within the territory controlled by the adversary, engaging the TBM during the boost phase is very difficult. The best chance for success is to attack the launcher facility before the TBM is launched. Once launched, there are no weapons currently in the U.S. inventory to successfully engage a TBM in the boost phase. In development is the Airborne Laser (ABL), whose primary mission is to engage boosting ballistic missiles with a chemical oxygen iodine laser (COIL) [18]. A kinetic interceptor is also in development, with an estimated fielding date of 2011 [18].

In the mid-course phase, there are two primary weapons that are available for intercept. For both mid-course weapons, a smaller “kill-vehicle” is launched to a predetermined release point by a booster. The kill-vehicle then maneuvers to intercept the TBM by impacting it directly [19]. The land based weapon is currently called the “Ground Based Interceptor”. The Standard Missile 3 (SM-3) is the sea-based interceptor that is launched from both Aegis destroyers and cruisers [19].

In the terminal phase, the TBM has returned to the earth’s atmosphere and is freely falling. Again, there are no HEL weapons currently used in this phase of the TBMs flight. Various kinetic weapons have been developed and fielded, including the Terminal High Altitude Area Defense System (THAAD), the Arrow, and the Patriot PAC-3.

B. DAMAGE REQUIREMENTS

Determining the damage requirements for a “kill” is difficult and time consuming. Proper lethality studies involve a component-by-component break down of a

Theater Ballistic Missile Defense Weapons		
Weapon	Type	Phase of Intercept
Airborne Laser	HEL	Boost Phase
RIM-161 (SM-3)	Kinetic	Mid-Course Phase
Ground Based Interceptor	Kinetic	Mid-Course Phase
THAAD	Kinetic	Terminal Phase
Arrow	Kinetic	Terminal Phase
PAC-3	Kinetic	Terminal Phase

Table II. TBMD Weapons

specific target. Each component is then analyzed for its ability, should it be destroyed, to cause the inbound missile to fail to damage its intended target. The mechanism for missing the target can be due to any of a number of causes, including the inbound missile losing lock on the target and not being able to reacquire, the loss of the missile’s ability to conduct aerodynamically stable flight, or the premature detonation of the missile’s warhead.

In the case of a ballistic missile, some kill mechanisms available to a TBMD system are ineffective. For example, a ballistic missile in the terminal phase that has lost its ability to “fly” aerodynamically will still likely impact within the intended target area. Ballistic missiles in the terminal phase are not flying so much as falling. Even with the removal of or significant damage to the nosecone, the missile will still continue close to its original ballistic path. Its horizontal and vertical velocities will be affected, but since, in the terminal phase, the TBM is essentially falling vertically (its horizontal velocity is much less than its vertical velocity) the result will be that the TBM falls at a slower velocity. Many TBMs have no terminal guidance to attack, again limiting the available kill mechanisms. As fuzing is typically highly redundant in expensive weapons, the ability of the TBM warhead to activate according to its fuze settings may not be easily affected.

To account for the difficulty in determining a definite kill mechanism, a simplified case is considered. A simple missile body with a unitary high explosive warhead,

situated immediately behind the nosecone is taken as our “typical” target. The kill mechanism will be burn-through of the exterior of the missile, causing heating of the explosive surface. As the explosive heats, the result will be deflagration, which will cause the explosive to be expended prior to impact in the intended target area. This methodology has been demonstrated against mortars and artillery rockets by the THEL program [20]. Supporting calculations will be shown in Section VI.B.3.

1. Missile Models

Theater ballistic missiles come in many sizes and have ranges from a few hundred kilometers to thousands of kilometers. To limit the intended target set for our high energy laser defense system, we only consider those missiles that have maximum ranges of less than 1,000 kilometers. Table (III) lists some example short and medium range TBMs and some pertinent information on size, payload, and country of origin.

Weapon Name	Range [km]	Payload [kg]	Country
CSS-5 Mod 2	2,500	Nuc (20, 90, 150 kT), Chem, Submunition, EMP	China
Taep'o-dong 1	2,000	750 - NBC & HE	North Korea
CSS-7 Mod 2	350-530	Nuc (2, 10, 20 kT) Chem, Submunition, HE, FAE	China
Scud 'C'	550	500 - HE	Iran
MGM-140 Blk 1A	300	160 - Submunition 213 - Unitary HE	USA
Tien Chi	120	90 - HE	Taiwan

Table III. Medium and short range TBMs [21]

2. Flight Patterns

All ballistic missiles go through the same phases of flight from launch to impact. The first phase is the boost phase, where the missile expends fuel to climb out

against gravity. Once above 10 km, where the atmospheric density has decreased by 63%, the missile begins to gain significant speed. After burn out of the rocket motor, the ballistic missile enters the mid-course phase. During mid-course, the missile may deploy decoy targets to confuse possible interceptors and detection schemes. After apogee, the ballistic missile begins to increase its velocity toward the ground under the influence of gravity. Upon reentry into the earth's atmosphere, the ballistic missile enters its terminal phase.

The primary differences between a short-range ballistic missile (SRBM) and an intercontinental ballistic missile (ICBM) are range, apogee altitude, re-entry velocity, and payload size. An SRBM can reach speeds of 2.2 km/sec at burnout and have a range of 500 km [22]. An ICBM can reach speeds of 5.7 km/sec at burnout and have ranges more than 10 times greater than an SRBM [22]. Apogee altitudes are also very different, with an ICBM tipping over at an altitude of 1200 - 1600 km [16] and an SRBM at 200 km [23, p. 27]. Figure (25) shows a relative comparison of the various ballistic missile flight paths.

Of interest to the terminal phase HEL defense is the time available for the laser to effect damage to the TBM. In the best case, most time available, the missile would be on a "direct hit" trajectory that presents the missile directly over the beam director. If we take a nominal light-on-target range of 30 km and assume a constant downward velocity of the TBM, then the HEL has from 6.7 to 20 seconds (4.5 to 1.5 km/sec TBM speed) before the missile impacts the intended target. If we say that the TBM must be defeated a minimum of 5 km above the defended ship, this reduces the engagement timeline to 5.6 to 16.7 seconds for the same TBM speeds.

3. Damage Methodologies

In this study, we only concern ourselves with the intercept of the TBM in its terminal phase. This greatly limits the avenues available to effect a kill of the incoming TBM. The first step is to consider how ruggedly the missile is constructed. At launch, the greatest amount of missile mass is taken up by the fuel. The desired

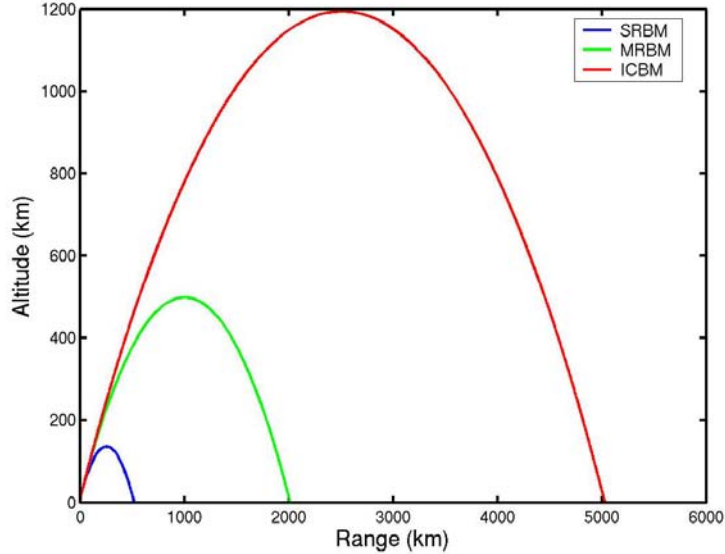


Figure 25. TBM flight paths generated numerically, allowing for altitude dependent drag and gravity. All TBMs are given an instantaneous impulse at 45° launch angle (no sustained burn) to achieve expected ranges.

range and throw weight (warhead size) determines how much fuel is necessary to move the TBM warhead to the target. The major structure of the missile must provide a stable flight platform for the rocket motor during boost, after that, it is additional weight that serves no purpose. After boost, the only structurally important component of the TBM is the reentry vehicle containing the warhead. The warhead section is the strongest part of the missile.

The warhead is

... built of the toughest metal alloys available, to withstand the physical stresses of reentry and to provide initial containment of explosions. Hence they are coated with heat shields the surfaces of which gradually flake off as they are burned away by air friction as they reenter the atmosphere. Warheads stand from six to nine feet tall, and weigh from a few hundred (for the most modern nuclear weapons) to a few thousand pounds [24].

If the body of the TBM is still attached, it provides no critical component that can be

targeted by a HEL. The primary components of interest are the high explosive warhead, targeting components - if any, and fuzes. As stated previously, most warheads are fuzed so that multiple fuze paths are available to the warhead to initiate detonation. This makes completely nullifying all fuze paths a daunting task in the little time available during a HEL engagement. The targeting components will be mounted safely behind the nose cone of the reentry vehicle to protect them from the heat of reentry. The successful defeat of the targeting components will not be apparent to the HEL platform until the TBM impacts – a successful engagement will not result in the detonation of the TBM. This is not a comforting situation for any warship to be in, leaving only the inducement of a detonation in the warhead explosive as the only definitive kill mechanism for the shipboard HEL.

Burn-through of the outer shell is achieved by directing the HEL onto a specific location on the missile body. The laser spot size should be large compared to the material’s ability to diffuse heat outside of the laser spot. This is described by defining a diffusion length, D , which must be smaller than the beam size,

$$D = 2\sqrt{\kappa t} \quad , \quad (\text{VI.1})$$

where κ is the thermal diffusivity,

$$t = \frac{\pi K^2 \Delta T^2}{4\mathcal{I}_0^2 \kappa} \quad , \quad (\text{VI.2})$$

K is the thermal conductivity, ΔT is the difference between ambient and the material melting temperature, and \mathcal{I}_0 is the incident irradiance [25, p. 22]. In general, if an intensity of 10 kW/cm² is incident over a 10 cm diameter spot, this condition is met for almost all materials. Table (IV) lists some materials and required spot sizes for \mathcal{I}_0 of 10 kW/cm².

The power deposited into the material surface is transformed into heat. As the temperature of the material rises, the material eventually melts, and the high speed air flow past the missile body causes the melted material to flow away from the targeted location. This melt removal assists the burn through process by removing

Material	Thermal Diffusivity (κ) [cm^2/s]	Thermal Conductivity (K) [$\text{W}/\text{cm K}$]	ΔT [K]	t [s]	Spot Size (D) [cm]
Aluminum	0.37	2.35	610	0.044	0.25
C-C Ceramic	0.0154	3.00	3030	42.1	1.61
Titanium Carbide	0.0659	0.272	2495	0.055	0.12
Sapphire	0.0051	0.172	2050	0.191	0.062
Diamond	2.00	4.00	3550	0.792	2.52

Table IV. Minimum spot size required for melt through of various materials for constant irradiance of $10 \text{ kW}/\text{cm}^2$

material that would otherwise have to be heated to the vaporization temperature. As an example, let us consider the amount of energy necessary to melt through two representative missile materials – aluminum and a generic carbon-carbon ceramic matrix. The fluence (energy per unit area) necessary to raise some thickness of material to its melting point is determined by

$$\mathcal{F} = \rho d [C_v (T_m - T_0) + \Delta H_m] \quad , \quad (\text{VI.3})$$

where \mathcal{F} is the fluence required for melt through, ρ is the density of the material, d is the thickness of the target material, C_v is the specific heat, T_m is the melting temperature of the material, T_0 is the initial temperature of the material, and ΔH_m is the latent heat of melting [10]. The time required to melt through the target can be determined by

$$t_{\text{melt-thru}} = \frac{\mathcal{F}}{P_{\text{incident}}} = \frac{\rho d [C_v (T_m - T_0) + \Delta H_m]}{\mathcal{I}_0} \quad . \quad (\text{VI.4})$$

Table (V) shows some common materials and the fluence required and time estimates for melt through.

Once the skin of the target has been removed, the HEL intensity is then applied to the explosive underneath. All explosives are sensitive to high temperatures, and through the application of high intensity laser light, the surface temperature of an explosive can be raised high enough to cause deflagration or high order detonation.

Material	ρ [g/cc]	C_v [J/gK]	T_m [K]	T_0 [K]	ΔH_m [J/g]	\mathcal{F} [J/cm ²]	$t_{\text{melt thru}}$ [s]
Aluminum	2.7	1.05	880	273	400	2,800	0.280
C-C Ceramic	3.0	0.9	3,300	273	1,600	13,000	1.30
Titanium Carbide	5.1	0.72	2,765	273	3,000	24,400	2.44
Sapphire	3.98	0.75	2,320	273	1,100	10,500	1.05
Diamond	3.515	0.51	3,820	273	59,000	214,000	21.4

Table V. Fluence required and melt-through times for various 1 cm slabs, with \mathcal{I}_0 of 10 kW/cm². Calculations assume perfect coupling between laser radiation and material.

If the outer surface of the explosive is in contact with the inner surface of the missile skin, heat transfer through the missile skin will raise the surface temperature close to the melting point of the skin material. In the case of aluminum, this is 600° C, far greater than temperatures required for deflagration for most explosives. If there is no direct contact between the explosive and the missile shell, the absorption of the laser light will quickly raise the temperature of the outer layers of the explosive above its deflagration temperature. In all cases studied, the deflagration time is considered coincident with burn through into the explosive.

4. TBMD Scenarios

Using the engagement modeling software, HELCoMES (**H**igh **E**nergy **L**aser **C**onsolidated **M**odeling and **E**ngagement **S**imulation), three different scenarios were modeled using the kill criteria developed in the previous section. HELCoMES is a scaling law model, meaning that the code is not a wave propagation code as we encountered in Chapter IV. However, HELCoMES uses data that has been gathered from wave propagation codes to estimate the spread of a laser beam’s energy as it propagates through a specified atmosphere. The fluence or power in a user specified “bucket” is then determined from this spread beam.

In these scenarios, a single ship with a HEL TBMD system installed is attacked with a single short range theater ballistic missile. The TBM is detected at launch

and tracked throughout its flight with appropriate cuing and track data being passed to the TBMD platform. Five scenarios were considered: the zenith attack, the short round attack (two ranges), and the lateral attack (two ranges). The zenith attack is a scenario where the TBM's impact point is the TBMD platform ship. The short round attack is a scenario where the missile's flight path takes it towards the TBMD ship, but the impact point will be short of the ship's position relative to the TBM's launch point. The lateral attack is a scenario where the TBM will impact at the same range (or greater) as the TBMD ship, but where the launch azimuth is such that its impact position will have lateral error. Both the lateral and short round scenarios are considered for displacements from the TBMD ship of 5 and 12 km. All scenarios are set up for laser light on target at a slant range of 30 km. Figure (26) shows a graphic of these engagements.

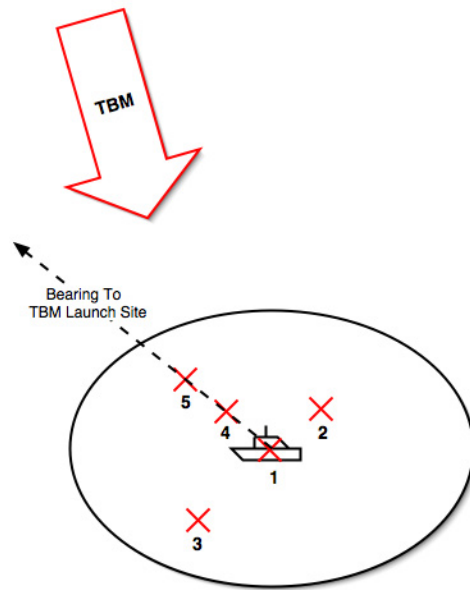


Figure 26. Considered scenario geometries. Impact 1 is the “zenith” scenario, impacts 2 and 3 are “lateral” scenarios, and impacts 4 and 5 “short round” scenarios.

In engaging the missiles in the various scenarios, the light will impinge at different points on the target. For the zenith scenario, the laser must bore through

the nosecone and the casing around the warhead before being able to apply laser light to the explosive. For the short round attack, the missile's flight path and attitude require burn through of the nose cone and the warhead casing as well. In the lateral engagement, the warhead section will be visible for both impact ranges considered. Propagation effects must also be considered, as there are great differences in the amount of absorption and scattering encountered between the zenith and the 12 km lateral and short round engagements.

To properly account for the different angles of attack on the inbound TBM, we must calculate the effective thicknesses of materials that the laser will need to burn through. Due to the high heat load on the nosecone of a TBM as it falls through the atmosphere, it must be made of a very heat resistant material. Since data on proprietary ceramics and other heat resistant materials are difficult to find, a generic carbon-carbon ceramic material will be substituted (see Table (V)). Since the skin of the missile must only provide structural support for the missile during flight, and its weight reduces the maximum effective range, we assume the skin of the missile is made of aluminum. Table (VI) lists the effective material thicknesses and fluence requirements for complete burn through to the explosive warhead.

Scenario	C-C Ceramic [cm]	Aluminum [cm]	\mathcal{F} [kJ/cm²]
1, fast	2.074	1.0	29.7
1, slow	1.992	1.002	28.6
2, fast	0	1.0	2.80
2, slow	0	1.0	2.80
3, fast	0	1.0	2.80
3, slow	0	1.0	2.80
4, fast	1.811	1.018	26.3
4, slow	1.760	1.028	25.7
5, fast	1.600	1.102	23.8
5, slow	1.572	1.126	23.5

Table VI. Burn through effective thicknesses and total fluence requirements

The HELCoMES program can be used to alter many different parameters affecting other portions of its model, such as tracker/illuminator parameters and adaptive optics parameters, that were not of interest to this study. For these input values, the defaults were accepted. As examples, the wavefront sensor and tracker frame rates were held at 500 Hz and had a quantum efficiencies of 0.8. These values are used to determine how effectively the optical system can compensate for atmospheric effects and target motion. In general, each engagement was modeled as a “Ship Defense” scenario in a dynamic environment. The dynamic environment allows for both the target and firing platform to move independently over a specified time period (usually up to the time of TBM impact). A circular shaped “bucket”, or target area, was used with a 10 cm diameter. The beam shape was a truncated Gaussian with a 1.5 m diameter director and a central obscuration of 0.25 m. The laser wavelength used was 1.045 microns, due to HELCoMES library considerations, and the output power was 5 MW. The platform was given a jitter of 3 μ rad. Adaptive optics were used to correct for turbulence effects. The atmosphere used was the Midlatitude Summer Navy with a 14.8 km visibility, shown in Figure (27), and a Clear 2 wind profile, shown in Figure (28). The turbulence profile used was the Maritime Hufnagle-Valley 5/7, shown in Figure (29).

Table (VII) shows the results from simulations for the fast TBM (4.5 km/s vertical speed) and Table (VIII) the slow TBM (1.5 km/s) results. Time of kill was determined by taking HELCoMES’ calculated target fluence at 0.5 sec intervals during the engagement and adding iteratively until the kill fluence was reached.

As can be seen in Tables (VII) and (VIII), the HEL is effective for both fast and slow targets when the impact point is very close to the firing unit. As a self defense weapon, this indicates that a HEL is quite effective. When close impact points are considered, approximately 5 km distant, the HEL is moderately effective. As the beam elevation angle decreases, the laser light must pass through more of the lower, more dense and turbulent atmosphere. The laser suffers even greater degradation

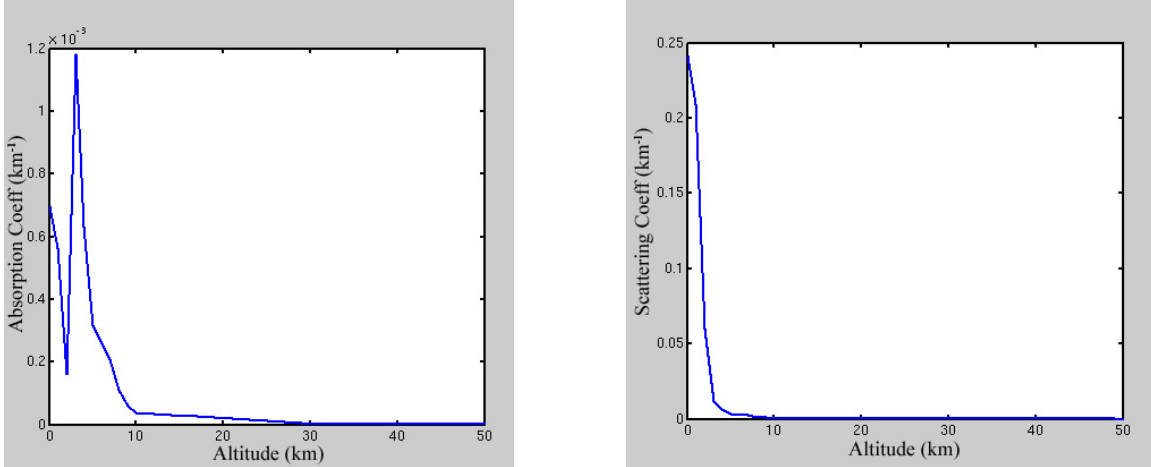


Figure 27. Midlatitude Summer Navy with 14.8 km visibility atmospheric absorption (left) and scattering (right) profiles

when the area defense scenarios are considered (12 km offset) as the elevation angle decreases even more. From HELCoMES output, the greatest contribution to inability to successfully engage the TBM is due to turbulence beam spread. Even when platform jitter is completely removed from the simulation, the HEL is unable to achieve 10 kW/cm^2 irradiance for the 12 km engagements, thus complete failure is assumed.

For the 5 km engagements, the 10 kW/cm^2 irradiance threshold is reached, but the laser must have sufficient time to apply the required kill fluence. For the fast TBM, the missile is moving fast enough so that it overcomes the benefits of a shorter slant range and the HEL is unable to apply enough fluence for a kill. In the slow cases, the HEL has a long enough engagement time that it can reach kill fluence. Unlike the 12 km offset case, if the platform jitter is removed, the average irradiance across the target bucket is increased sufficiently to achieve a kill, even in the fast TBM case.

To determine the minimum power necessary to successfully engage a TBM in a purely self-defense mode, i.e. zenith attack, the zenith scenarios were run with the same parameters with successively smaller output powers until the kill fluence could not be achieved with a minimum kill distance from the ship of 5 km. The result is

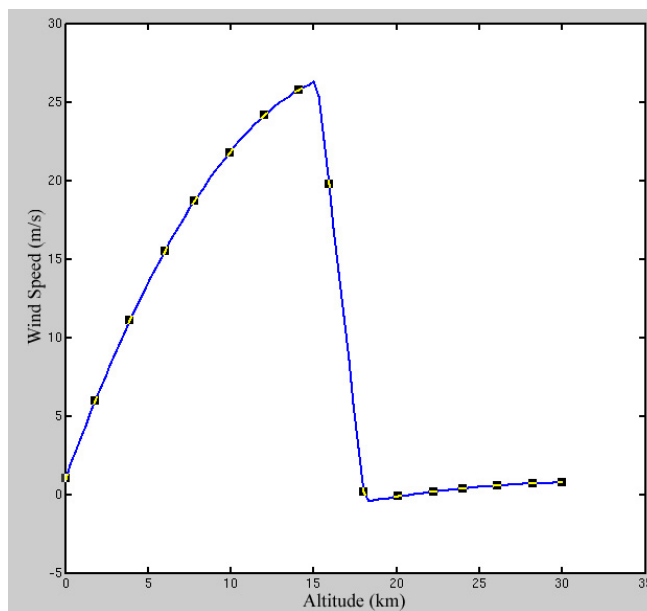


Figure 28. Clear 2 wind profile

that a minimum of 1 MW output power is necessary for the slow target and 2 MW for the fast target. Since one creates a design based upon worst case scenarios, should the HEL target set include TBMs, then a minimum output of 2 MW is necessary.

Scenario	Time to Reach 10 kW/cm ² [s]	Kill Altitude [km]	Time to Kill [s]
1	2.1	9.0	4.0
2	3.9	fail	fail
3	fail	fail	fail
4	4.0	fail	fail
5	fail	fail	fail

Table VII. Fast TBM intercept results

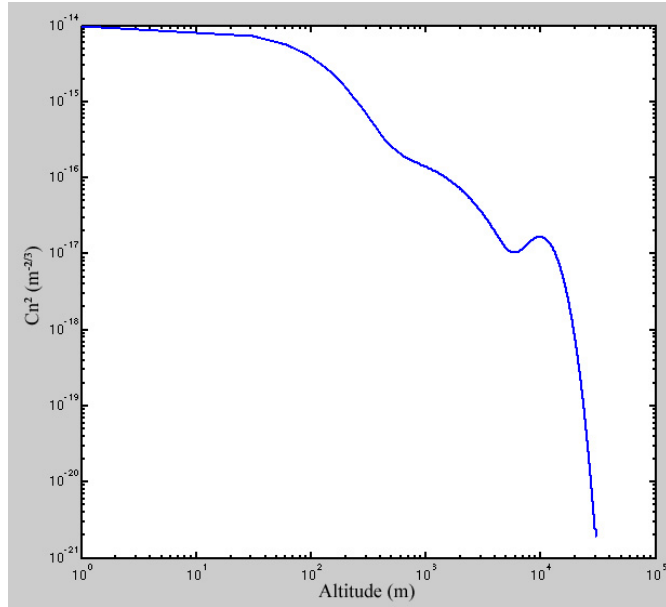


Figure 29. Maritime Hufnagle-Valley 5/7 turbulence profile

Scenario	Time to Reach 10 kW/cm ² [s]	Kill Altitude [km]	Time to Kill [s]
1	8.0	14.0	10.0
2	5.15	20.4	6.0
3	fail	fail	fail
4	6.5	13.7	10.0
5	fail	fail	fail

Table VIII. Slow TBM intercept results

C. CONCEPT OF OPERATIONS FOR TMBD LASER

As with any new weapon, a general understanding of the capabilities and limitations of the system must be developed to ensure that it is properly employed. In the case of a HEL TMBD system, the decision to engage a target has many consequences that depend upon the warhead trajectory, warhead type, and whether the system is being used in a self-defense or area-defense mode.

1. Engagement Criteria

The decision to fire is one of the most important that can be made by the commander at sea. In a situation where the threat of TBM attack is present, there will most likely be ample warning that a threat is inbound. This is unlike a cruise missile attack where the threat can just appear on the horizon. The time available will probably allow the strike group commander time to set up a defense in depth.

a. Time Line

Assuming that all planned TBMD assets are available to the theater commander, a generalized detect-to-engage scenario would proceed along fairly similar lines to those of other weapon systems. The TBM launch will be detected through space-based sensors, either by infrared detection of the thermal signature of launch or by radar tracking. An alert based upon TBM track will be given to units that can engage or should prepare for impact in the theater. An Airborne Laser, if available will attempt to engage the missile as it rises in the boost phase. Failing this, the engagement will be passed to a mid-course engagement system, most likely a sea-based one for a sea-based impact point. A salvo of kinetic interceptors would be launched against the TBM, however given the relative speed of the TBM, there will not be time for a re-engagement with kinetic weapons should the interceptors fail.

Once mid-course engagement options have been exhausted, the strike group and unit commanders who have TBM capable HEL systems will be the last line of defense. Because of the cuing involved in a TBM engagement, units in the impact area will have ample time to prepare for the engagement, including standard

general quarters preparations.

b. Geometry Considerations

The geometry of an engagement has significant impact on the length of time the engagement requires. The greater the fluence required to burn through to the sensitive missile components, the longer the engagement last for a given incident power. As the required engagement time increases, it becomes less likely that the TBM will be defeated at an altitude to minimize damage to friendly forces.

Unlike missile engagements, the crossing shot is the best geometry for a HEL intercept. By unmasking the warhead section of the TBM, the fluence requirements to burn through the missile skin are significantly reduced. This creates a situation where the best defense for a ship may be another ship to engaging the inbound TBM. For this to be effective, all HEL platforms will need to have highly accurate track data that can be shared quickly and efficiently.

As the pointing angle approaches zenith, the lower the absorption and blooming effects, as the more dense and absorptive portions of the atmosphere are minimized along the propagation path. However, this geometry reintroduces the additional fluence required to burn through the nose cone in a self-defense mode. Again, the best ship defense in this case is a cooperative engagement by another HEL equipped ship with a more favorable engagement geometry.

c. Warhead Targeting

The conventional unitary warhead presents the least difficult target of the possible engagement possibilities. Given a specific missile type, the warhead position in the missile is known and a pre-determined offset can be inserted into the targeting/pointing mechanism. A favorable geometry would allow for burn through of the missile skin into the warhead section without the need of burning through more energy-absorbing missile sections.

For more difficult warhead types, such as nuclear, biological, chemical, electromagnetic pulse, or explosive submunitions, some knowledge of the missile launched and its configuration would be necessary to target the missile in the most

advantageous section of the missile body. Without this knowledge, the nonexplosive warheads will give no indication of a successful engagement other than the failure of their warhead to impart the desired effect. Even in the explosive submunition case, total success may not be possible and the detonation of one submunition may cause the other submunitions to scatter, creating many small ballistic targets. Other warhead types may have the same drawbacks to engagement, such as greater dispersion of the chemical or biological agent. Further study is definitely warranted to develop adequate engagement tactics against these type warheads.

2. Self-Defense Considerations

In the event that the TBM is predicted to impact an HEL-equipped ship, it makes sense and is expected that a ship commander would engage in self-defense. Even in a case where the outcome could be predicted to be hopeless, a commander would be remiss if he did not pursue even the remote chance of success by engaging the target. If the point of impact is the HEL ship, geometry considerations imply no advantage to waiting, and the TBM should be engaged at the greatest range possible. As there is a remote chance that laser light on target at greater than 30 km may cause some malfunction that would effectively kill the TBM, it would be foolish not to try.

3. Area Defense Considerations

We have seen from our HELCoMES simulations that a 5 MW HEL was not effective in engaging targets with an impact point beyond 5 km from the HEL equipped ship. This implies that a single vessel will not be capable of providing a TBM defense umbrella beyond the immediate waters around itself. As strike groups operate, they arrange screening formations of combatant ships around the high value units to protect them from attack while carrying out their missions.

In the case of an aircraft carrier, it is reasonable to expect that a HEL equipped ship would be assigned as a close escort. In the event of a TBM attack that would impact close to the high value unit, this escort ship, if properly placed in its screen,

could provide some measure of additional defense. To be most effective against a TBM, the screening ship should be placed along a line perpendicular to the threat access. This places the screening asset in a position where threats that are inbound on the high value unit can be engaged from the side, providing the most advantageous geometry for kill with an HEL. This screening set up also allows the screening unit to engage cruise missiles with the same advantageous geometry as well. Unfortunately, this type of screening position is the least desirable for kinetic weapons that could also be used in such engagements.

4. Weapon Readiness Conditions

As with all weapons aboard naval ships, a weapon readiness matrix will be necessary to ensure the availability of this weapon to perform its mission. In general terms, for those not familiar with the conditions of weapons readiness, the following descriptions are provided. Condition IV is the lowest condition of readiness, usually reserved for peacetime steaming. Condition III provides for the next longest time to readiness to fire and usually means that many of the safety mechanisms to prevent accidental firing are still in place. Condition II means that only a few safety mechanisms remain in the firing train to prevent use of the weapon. Condition I is used when the use of the weapon may be necessary at short notice and implies that there may only be one safety interlock remaining in the firing chain. Using a service pistol as an example: condition IV would be having weapons available for issue to watch standers in the armory; condition III would be watch standers armed with loaded magazines, but no magazine inserted in the weapon; condition II would move to the insertion of the magazine into the pistol, but no round chambered; condition I would be a round chambered and only the weapon's safety preventing the use of the weapon.

The readiness conditions for a TBMD HEL weapon would be dependent upon the type of HEL that was installed. For the purposes of this discussion, a FEL will be assumed as our baseline system. In condition IV, the only systems that would need to remain online would be the liquid helium cooling systems. The usefulness

of the optical systems for other watch standing needs may mean that these systems would remain online at all times. In condition III, RF power would be applied to the accelerator modules, providing accelerating power for electrons should they be needed, but the electron beam would not be on. A small current beam may be used to “tune-up” alignment of magnets and resonator mirrors. Conditions II and I would essentially be the same, as the only remaining step necessary to put light out of the machine would be the application of a high current beam of electrons through the wiggler. The primary difference would be to occasionally pass a single electron bunch during condition II to validate the accelerator alignment without lasing. In condition I, the bunches could be more frequent by a factor of 100 or 1000, but since only milliseconds are necessary for the FEL to lase at full power, the final step before putting light on target is to turn the electron gun on at its full duty cycle.

One advantage to a HEL being used aboard ship is that the timeline can be compressed significantly over a kinetic weapon. With a kinetic weapon, the decision to put ordance on target must take into consideration fly-out time and intercept evaluation. With a HEL, once the order is given, the lasing mechanism only takes a fraction of a second to generate light, which is propagated to the target essentially instantaneously. Intercept can be constantly monitored until it is determined that the target has been killed, otherwise, the laser remains on target and continues to deliver power.

D. ADDITIONAL BENEFITS

The installation of a HEL for TBMD aboard a Navy ship brings other systems that are useful to the crew. The light that is issued from the beam director does not necessarily have to be applied to ballistic missiles only. Nothing prevents a TBMD system from being used against other surface or airborne targets. Perhaps the most interesting use for a HEL system aboard ship would be the optics used to send the beam to the target.

1. Optical Uses

The optical systems for a HEL must be of the highest quality possible. Inserting optical or infrared detection systems into the beam line when the HEL is not in use provides the ship with an excellent, gimballed (stable) platform to gather intelligence about targets of interest. In the typical Combat Information Center (CIC), the largest hindrance to maintaining situational awareness is the lack of ability to “see” what is going on. The typical CIC watch stander is inundated with radar and EW information, but must rely upon the lookouts and bridge watchstanders for visual information.

Having an optical system that can be slewed quickly to a radar contact, and being able to gather information from many portions of the spectrum (visible, IR, etc.) gives the individual CIC watchstander the ability to quickly identify and classify unknown targets.

2. Sea Skimming Cruise Missile Defense

The idea of placing a HEL system aboard ship for cruise missile defense has already been explored. The primary reason for the shorter ranges considered in this application is due to the curvature of the earth and the fact that the engagement geometry is horizontal. This horizontal beam path keeps the beam in the most absorptive and scattering portion of the atmosphere for the beam’s entire propagation length. In some geometries, increasing the power of the beam only speeds the onset of thermal blooming, defeating the attempt to apply greater power to the target.

Most HEL systems are able to provide variable output power. A system designed for TBMD, with a greater maximum output power can be “dialed down” to provide light for a cruise missile engagement with the same effectiveness as a system specifically designed for this mission. If the system is wavelength-tunable, as with a FEL, the system could also be tuned to use different wavelengths depending on the application for which it is to be used.

3. Small Craft Swarm Defense

One of the more worrisome engagements that face the naval surface fleet today is that of a swarm of small surface craft. Currently installed systems such as the Close in Weapon System (CIWS), small arms (MA-2 .50 caliber and M-60 machine guns), and missile systems are not optimal to counter this threat. Small arms and CIWS are very range limited and allow the small craft to approach dangerously close before they can be effectively engaged. Missile systems can reach out further, but are a very expensive method that cannot be employed arbitrarily close to one's own ship. In addition, the defending ship must wait until the rounds reach the incoming threat in order to determine a successful kill. A HEL gives a weapon that can be applied at range and continuously without regard to an ammunition supply.

Unfortunately a HEL system will suffer the same issue that current systems have in targeting swarming small craft on the ocean surface. The ocean surface is a highly cluttered environment in which it is difficult to rely upon radar tracks. However, as discussed previously, with the addition of other wavelength detectors coincident to the HEL beam path, it may be possible to use IR or optical guidance to target these small craft.

THIS PAGE INTENTIONALLY LEFT BLANK

VII. CONCLUSION

There are many considerations that must be explored to put a high energy laser system onto a surface combatant. The benefits that are implied in the technology certainly justify the expenditure of funds and effort necessary to continue to develop the systems and explore the tactics and applications.

Lasers involve sensitive optical systems and their performance is highly dependent upon the performance of the materials incorporated. Unfortunately, as power levels increase, our understanding of the material interactions that occur at high irradiance are not as developed. As high power lasers become more available for study, this should improve. A significant gap in understanding the use of a HEL as a weapon system is in the largest piece of the optical train – the atmosphere. Models have been developed to describe and predict water and aerosol size and concentration in certain situations. However not all the models agree and their ability to predict in “good” weather can only be described as fair. Further study needs to be devoted in this arena, especially in the maritime and littoral environment, if a HEL weapon is to be placed aboard ship.

The proliferation of theater ballistic missiles to non-friendly nations indicates that the armed forces will be facing these threats more often in future conflicts. The United States has already begun developing ballistic missile defenses and continues to do so. As the focus of the US Navy continues to move from the open ocean to the littoral environment, their assets afloat are brought within the engagement ranges of TBMs. At present, the Navy has developed the ability to intercept TBMs in the mid-course phase. The Army has developed multiple systems to handle ballistic missiles in the terminal phase, but Navy ships of a Carrier Strike Group or Expeditionary Strike Group are essentially defenseless should a mid-course engagement fail. The Navy already desires the ability to engage cruise missiles with a HEL weapon. This study has shown that a 5 MW output power capable HEL system in a self-defense role may be

also capable of engaging and defeating theater ballistic missiles in the terminal phase. Further study is necessary to fully explore the complete warhead target set, including nuclear, biological, chemical, electro-magnetic pulse, and submunitions. Also, the kinetics of a TBM as it reenters the atmosphere should be explored to determine if a spin-stabilized or tumbling warhead would increase laser dwell times sufficiently to render a HEL defense impractical.

APPENDIX A. CODE

Listed in this appendix are the wave propagation code used to simulate atmospheric effects. The graphics in the text were made using MatLab, and an example .m file for displaying the simulation results is included. Additionally, the .m file used to analyze the beam wander data is included.

1. WAVE PROPAGATION CODE

```
/* turb11.c : Models the propagation of a laser beam in the atmosphere
   from beam director to target. This simulation takes
   into account atmospheric turbulence.
```

```
    LT Sean Niles
    PH 4911
    May 2004                */
```

```
/* Compiler Instructions */
```

```
#include<stdio.h>
#include<math.h>
#include<stdlib.h>
#include<time.h>
```

```
/* Constants */
#define PI 3.14159265359
```

```
/* Function Declarations */
```

```
void BeamPlotter (int nx, float time, float array1[] [],
float array2[] [], int printType, FILE *filename);
void CtrFinder (int nx, float window, float array1[] [],
float array2[] [], float energy, FILE *filename);
```

```
int main(void)
```

```
{
```

```
/* Independent Variable Declarations */
```

```
float tau = 0.0;           // Dimensionless time (0 -> 1)
int x = 0;                 // Lateral distance from beam center
int y = 0;                 // Vertical distance from beam center
float radius2 = 0.0;      // Radial distance from beam center
```

```

//      (x^2 + y^2)
float waist = 0.0;          // Waist size of beam
float dx = 0.0;            // X bin element size
float phi = 0.0;          // Radial angle
float dPhi = 0.0;         // Change due to atmospheric effects
float energy = 0.0;       // Current time step wave energy
float energyInit = 0.0;   // Initial energy of wave
float ETarget = 0.0;     // Energy deposited in target area
float dt = 0.1;          // Time step
float r1 = 0.1;          // Random Number
float r2 = 0.1;          // Random Number
float temp = 0.0;        // Holder for lensing operator
int hit = 0;             // Counts whether the lensing effect has
// already been accounted for
int done = 1;           // Sorting switch
int count = 0;
int i, j, iter, scrnComp;

FILE *input, *E, *tauC, *screenVals, *ampData, *initial, *final,
*output, *irr, *spread;
input = fopen("light.in", "r");
output = fopen("output.txt", "w");
irr = fopen("center2.out", "w");
spread = fopen("center1.out", "w");
E = fopen("energy.out", "w");
tauC = fopen("tauc.in", "r");
//tauC = fopen("tauc.out", "w");
screenVals = fopen("screens.out", "w");
ampData = fopen("ampData.out", "w");          // type 1 for beam plotter
initial = fopen("initialAmp.out", "w");      // type 2 for beam plotter
final = fopen("finalAmp.out", "w");          // type 3 for beam plotter

/* User Input Variable Declarations */
float C = 0.0;          // Numerical Coefficient
float a0 = 0.0;        // Amplitude of initial wave form
float z0 = 0.1;        // Raleigh length
float winWidth = 1.0;  // Transverse window width
int numElements = 1;   // Number of x, y elements
float tauWaist = 0.0;  // Dimensionless time of beam waist
float k0 = 2.0;        // Turbulent Field wavenumber
float phiBend = 0.0;   // Bending lens strength
float phiLens = 0.0;   // Focus/Defocusing lens strength

```

```

float phiBloom = 0.0; // Thermal blooming lens strength
float phiTurbulence = 0.0; // dPhase strength due to atmospheric
// turbulence
int iterations = 0; // Number of iterations to perform
int kDistType = 1; // Distribution type to be used for making
// screens
int numScreens = 0; // Number of screens to use in simulation
int numScreenComponents = 0; // Number of components in each screen
int seed = 1; // random number seed

fscanf(input, "%f %f %f %f", &C, &a0, &z0, &winWidth);
fscanf(input, "%d %f %f", &numElements, &tauWaist, &phiBend);
fscanf(input, "%f %f %f", &phiLens, &phiBloom, &phiTurbulence);
fscanf(input, "%f %d %d", &k0, &iterations, &numScreens);
fscanf(input, "%d %d %d", &numScreenComponents, &kDistType, &seed);
fclose(input);

/* Variable Initalizations */
waist = sqrt(1 + (tauWaist * tauWaist / (z0 * z0)));
dx = winWidth / (float)numElements;
//srand(seed);
scrnComp = 0;

/* Initialize random number sequence */
int utime;
long ltime;
ltime = time(NULL);
utime = (unsigned int) ltime/2;
srand(utime);

/* Generate Random Screens for turbulence */
float tau_C [numScreens + 1]; // Time of atmospheric
// interaction
float screen [numScreens][numElements][numElements]; // Phase Screens
float r3[numScreenComponents]; // Random Number (rotation)
float k[numScreenComponents]; // Exponential fourier components
// for turbulence
float kx[numScreenComponents]; // x-direction component
float ky[numScreenComponents]; // y-direction component

/* Beginning of Iteration Loop */
for (iter = 1; iter <= iterations; iter++)

```

```

{
dt = 4.0 * C * dx * dx;
energy = 0.0;
hit = 0;

fprintf(output, "\nIteration #%d\t dt:%f\tC:%f\t\n", iter, dt, C);
printf("\nIteration #%d\t dt:%f\tC:%f\n", iter, dt, C);

if (scrnComp < iter)
{
for(i = 0; i < numScreens; i++)
{
fscanf(tauC, "%f", &tau_C[i]);
}
tau_C[numScreens] = 2.0;    // Final screen position outside of t
// considered

// Put screen times in ascending order
while (done != 0)
{
done = 0;

for (i = 0; i < numScreens; i++)
{
if ( tau_C[i] > tau_C[i + 1])
{
temp = tau_C[i];
tau_C[i] = tau_C[i + 1];
tau_C[i + 1] = temp;
done ++;
}
}
} // end of sorting while loop

temp = 0.0;

fclose(tauC);

/*****
***** SCREEN GENERATION SECTION *****/
*****/

```

```

// generate screens
for (j = 0; j < numScreens; j++)
{
for (i = 0; i < numScreenComponents; i++)
{
r1 = rand() / (float) RAND_MAX;
    while (r1 < 0.000001) r1 = rand() / (float) RAND_MAX;

r2 = rand() / (float) RAND_MAX;
r3[i] = rand() / (float) RAND_MAX;

if (kDistType == 1) // Exponential Distribution
{
k[i] = -k0 * log(r1);
}

if (kDistType == 2) // k(-6/5) Distribution
{
k[i] = k0 * pow(r1, -6.0 / 5.0);
}

kx[i] = k[i] * cos(2.0 * PI * r2);
ky[i] = k[i] * sin(2.0 * PI * r2);
}

for (y = 0; y < numElements; y++)
{
for (x = 0; x < numElements; x++)
{
dPhi = 0.0;

for (i = 0; i < numScreenComponents; i++)
{
dPhi += sin((kx[i] * ((float) x -
(numElements / 2.0) + 0.5)) +
(ky[i] * ((float) y -
(numElements / 2.0) + 0.5)) +
(2.0 * PI * r3[i]));
}

screen[j][x][y] = dPhi / (numScreens *
numScreenComponents); // Scaled Version

```

```

fprintf(screenVals, "%8.7f\t", dPhi);
}

fprintf(screenVals, "\n");
}

fprintf(screenVals, "\n");
} // end of screen generation

fclose(screenVals);
fprintf(output, "Screens generated\n");
printf("Screens generated\n");

scrnComp++;
} // end of screen if stmt

float aReal[numElements][numElements]; // Real part of amplitude
// matrix
float aImagine[numElements][numElements]; // Imaginary part
float aRealOld[numElements][numElements]; // Previous real
// iteration
float aImagineOld[numElements][numElements]; // Previous imaginary
// iteration

for (x = 0; x < numElements; x++) for (y = 0; y < numElements; y++)
{
    aReal[x][y] = 0.0;
    aImagine[x][y] = 0.0;
    aRealOld[x][y] = 0.0;
    aImagineOld[x][y] = 0.0;
} // end of clearing loop

/* Initial Optical Wave Form */
for (x = 0; x < numElements; x++) for(y = 0; y < numElements; y++)
{
    radius2 = (pow(x - (numElements / 2.0) + 0.5, 2.0) + pow(y -
        (numElements / 2.0) + 0.5, 2.0)) * dx * dx;
    phi = -radius2 * tauWaist / ((z0 * z0) + (tauWaist * tauWaist));

    aReal[x][y] = (a0 / waist) * exp((-radius2) / (waist * waist *
        z0)) * cos(phi);
    aImagine[x][y] = (a0 / waist) * exp((-radius2) / (waist *

```

```

        waist * z0)) * sin(phi);

    energy += (aReal[x][y] * aReal[x][y]) + (aImagine[x][y] *
aImagine[x][y]);
} // end of initialize loop

energyInit = energy;
fprintf(E, "%f\t%f\n", tau, energy);
fprintf(output, "beam initialized\n");
printf("Beam intialized \n");

//Print initial print shape
BeamPlotter (numElements, tau, aReal, aImagine, 2, initial);
fclose(initial);

//Print beam size
CtrFinder (numElements, winWidth, aReal, aImagine, energy, spread);
fclose(spread);

/*****
***** PROPAGATION SECTION *****/
*****/

/* Propogation Loop */
for (tau = dt; tau <= 1.0; tau += dt)
{
    // Reset Variables
    energy = 0.0;

    // Make Old value matrix the same as initial
    for (x = 0; x < numElements; x++)
    {
        for (y = 0; y < numElements; y++)
        {
            aRealOld[x][y] = aReal[x][y];
            aImagineOld[x][y] = aImagine[x][y];
        }
    }
} // end of new -> old changes

// Equations of Motion

```

```

    for (x = 1; x < numElements -1; x++)
    {
        for (y = 1; y < numElements -1; y++)
        {
            aReal[x][y] += -C * (aImagineOld[x+1][y] +
aImagineOld[x-1][y] +
                                aImagineOld[x][y+1] + aImagineOld[x][y-1] -
                                (4.0 * aImagineOld[x][y]));
            aImagine[x][y] += C * (aRealOld[x+1][y] + aRealOld[x-1][y]
+ aRealOld[x][y+1] + aRealOld[x][y-1] -
                                (4.0 * aRealOld[x][y]));
        }
    } // end of update loop

/***** LENS SECTION *****/
/*****

// check for bending lens effects
if ((phiBend > 1.0E-5) && (tau >= tau_C[hit]))
{
for (x = 0; x < numElements; x++)
{
for (y = 0; y < numElements; y++)
{
dPhi = 0.0;
dPhi = phiBend * (x - (numElements / 2.0) + 0.5);

temp = aReal[x][y];
aReal[x][y] = (aReal[x][y] * cos(-dPhi)) -
(aImagine[x][y] * sin(-dPhi));
aImagine[x][y] = (temp * sin(-dPhi)) +
(aImagine[x][y] * cos(-dPhi));
} // end of y
} // end of x

hit ++;
} // end of bending lens

// check for focusing lens effects

```

```

if ((phiLens > 0.001 || phiLens < -0.001) && tau >= tau_C[hit])
{
for (x = 0; x < numElements; x++)
{
for (y = 0; y < numElements; y++)
{
dPhi = 0.0;

radius2 = (pow(x - (numElements / 2.0) + 0.5, 2.0) +
pow(y - (numElements/ 2.0) + 0.5, 2.0)) * dx *
dx;

dPhi = radius2 * phiLens;

temp = aReal[x][y];
aReal[x][y] = (aReal[x][y] * cos(-dPhi)) -
(aImagine[x][y] * sin(-dPhi));
aImagine[x][y] = (temp * sin(-dPhi)) +
(aImagine[x][y] * cos(-dPhi));
} // end of y
} // end of x

hit ++;
} // end of focusing lens

// check for thermal blooming lens effects
if ((phiBloom > 1.0E-5) && (tau >= tau_C[hit]))
{
for (x = 0; x < numElements; x++)
{
for (y = 0; y < numElements; y++)
{
dPhi = 0.0;

dPhi = (pow(aReal[x][y], 2.0) +
pow(aImagine[x][y], 2.0)) * phiBloom;

temp = aReal[x][y];
aReal[x][y] = (aReal[x][y] * cos(-dPhi)) -
(aImagine[x][y] * sin(-dPhi));
aImagine[x][y] = (temp * sin(-dPhi)) +

```

```

(aImagine[x][y] * cos(-dPhi));
} // end of y
} // end of x

hit ++;
} // end of thermal blooming lens

// check for turbulence lens effects
dPhi = 0.0;

// Turbulence
if ((phiTurbulence > 0.00001) && (tau >= tau_C[hit]))
{
    for (x = 0; x < numElements; x++)
    {
        for (y = 0; y < numElements; y++)
        {
            dPhi = 0.0;

            dPhi = screen[hit][x][y] * phiTurbulence;

            temp = aReal[x][y];
            aReal[x][y] = (aReal[x][y] * cos(-dPhi)) -
(aImagine[x][y] * sin(-dPhi));
            aImagine[x][y] = (temp * sin(-dPhi)) +
(aImagine[x][y] * cos(-dPhi));
        }
    }

    hit ++;
} // end of turbulence

// Check for energy conservation
for (x = 0; x < numElements; x++) for (y = 0; y < numElements; y++)
{
    // Calculate energy in wavefront
    energy += (aReal[x][y] * aReal[x][y]) + (aImagine[x][y] *
aImagine[x][y]);
} // end of wavefront calculation

// Print cross-section of beam

```

```

    if (tau >= (float) count / 500.0)
    {
        BeamPlotter (numElements, tau, aReal, aImagine, 1, ampData);
        fprintf(E, "%f\t%f\n", tau, energy);
count++;
    }

    if (pow(100.0 * (energyInit - energy) / energyInit, 2.0) > 25.0)
    {
        iter--;
        C = C / 2.0;
        fprintf(output, "Energy not conserved.\n");
        fprintf(output, "tau\t%f\tnew C: %f\tE/E\t%f\n", tau, C,
            100.0 * (energyInit - energy) / energyInit);
        printf("Energy not conserved\n");
        printf("tau\t%f\tnew C: %f\tE/E\t%f\n", tau, C, 100.0 *
            (energyInit - energy) / energyInit);

        tau = 2.0;
count = 0;

        // reset output files
        initial = fopen("initialAmp.out", "w");
        fclose(ampData);
        ampData = fopen("ampData.out", "w");
        fclose(final);
        final = fopen("finalAmp.out", "w");
fclose(E);
E = fopen("energy.out", "w");
    }
} // end of time loop

// Print final beam cross-section
BeamPlotter (numElements, tau, aReal, aImagine, 3, final);
fclose(final);

/* Plot position of beam center & final beam width if energy conserved*/
if (pow(100.0 * (energyInit - energy) / energyInit, 2.0) <= 25.0)
{
    CtrFinder (numElements, winWidth, aReal, aImagine, energy, irr);
    fprintf(output, "Iteration %d complete\n", iter);
    printf("Iteration %d complete\n", iter);
}

```

```

}

} // end of iteration loop

fprintf(output, "Run Complete\n");
printf("Run Complete\n");
fclose(E);
fclose(output);
//fclose(ampData);
return(0);
} // end of main

/*=====
Beam Amplitude Plotter: Output generator
=====*/
void BeamPlotter (int nx, float t, float aReal[nx][nx],
float aImagine[nx][nx], int dataType, FILE *fileName)
{
    int x, y;

    switch (dataType)
    {
        case 1:          // Propogation Amplitude Data
// (slice from tau 0->1)
        {
            for (x = 0; x < nx; x++)
            {
                fprintf(fileName, "%f\t",
sqrt(pow(aReal[x][(int)nx/2], 2.0) +
pow(aImagine[x][(int)nx/2], 2.0)));
            } // end of for

            fprintf(fileName, "\n");

            break;
        } // end of case 1

        case 2:          // Initial Amplitude Plot
        {
            for (y = 0; y < nx; y++)
            {
                for (x = 0; x < nx; x++)

```

```

        {
            fprintf(fileName, "%f\t",
sqrt(pow(aReal[x][y], 2.0) +
            pow(aImagine[x][y], 2.0)));
        } // end of for

        fprintf(fileName, "\n");
    }

    break;
} // end of case 2

case 3:      // Final Amplitude Plot
{
    for (y = 0; y < nx; y++)
    {
        for (x = 0; x < nx; x++)
        {
            fprintf(fileName, "%f\t",
sqrt(pow(aReal[x][y], 2.0) +
            pow(aImagine[x][y], 2.0)));
        } // end of for

        fprintf(fileName, "\n");
    }

    break;
} // end of case 3

default:
    fprintf(fileName, "No Data to Output");
} // end of switch

return;
} // end of Beam Plotter

/*=====
CtrFinder(): Finds the center of irradiance at the target to measure
and plot beam centroid wander
=====*/

void CtrFinder (int nx, float win, float R[nx][nx], float I[nx][nx],

```

```

float energy, FILE *out)
{
    int x, y;
    float irradiance = 0.0;          // Irradiance value
float irr_tot = 0.0; // Total irradiance on final screen
float x_irr = 0.0; // x Position weighted by irradiance
float y_irr = 0.0; // y Position weighted by irradiance
    float high = 0.0;              // Value of greatest irradiance
    float x_pos = 0.0;            // x Position of the irradiance
    // maximum
    float y_pos = 0.0;            // y Position of the irradiance
// maximum

float bm_rad = 0.0; // radius of energy integration for
// spreading
float intEnergy = 0.0; // integrated energy
float radius = 0.0;

    for (x = 0; x < nx; x++) for (y = 0; y < nx; y++)
    {
        irradiance = R[x][y] * R[x][y] + I[x][y] * I[x][y];

        if (irradiance > high) high = irradiance; // check for peak

x_irr += (win / (float) nx) * ((float) x - (nx / 2.0) + 0.5) *
irradiance;
y_irr += (win / (float) nx) * ((float) y - (nx / 2.0) + 0.5) *
irradiance;
irr_tot += irradiance;
    }

x_pos = x_irr / irr_tot;
y_pos = y_irr / irr_tot;

while (intEnergy <= 0.8 * energy)
{
bm_rad += win / (float) nx;
intEnergy = 0.0;

for (x = 0; x < nx ; x++) for (y = 0; y < nx; y++)
{
radius = sqrt(pow(x_pos - (win / (float) nx) * ((float) x -

```

```

(nx / 2.0) + 0.5), 2.0) +
pow(y_pos - (win / (float) nx) * ((float) y -
(nx / 2.0) + 0.5), 2.0));
irradiance = R[x][y] * R[x][y] + I[x][y] * I[x][y];

if ((radius <= bm_rad) && (bm_rad < win / 2.0))
intEnergy += irradiance;

} // end of screen run through

if (bm_rad > win / 2.0) intEnergy = 9E9;

} // end of radius finder

    fprintf(out, "%f\t%f\t%f\t%f\n", x_pos, y_pos, bm_rad, high);

    return;
} // end of Center Finder

```

2. BEAM ANALYSIS

%plotter.m : Displays the output data from a single beam propagation

```

close all, clear all;
load ampData.out;
load finalAmp.out;
load initialAmp.out;
load screens.out;

figure(1);
pcolor(initialAmp);
shading flat; shading interp;

figure(2);
pcolor(finalAmp);
shading flat; shading interp;

figure(3);
pcolor(ampData');
shading flat, shading interp;

```

```
%Turb_Curve.m Plot the standard deviation of the beam wander as a
%function of turbulence strength. In this case, only a screen k of 0.01 is
%considered.
```

```
close all, clear all;
```

```
% User Inputs
```

```
lambda = 1.064E-6;           % wavelength of light (m)
range = 10E3;                % Propagation Distance (m)
z0_n = 1.0 * range;         % Rayleigh range (m)
```

```
dim_coeff = sqrt(range * lambda / pi);
coeff_long = (z0_n * lambda / pi)^(1/6) / (1.44 * range^3);
```

```
current_dir = cd;
```

```
x1 = [0,50,100,150,200,250,300,350,400,450,500]; % k0_0.01
```

```
%%%%%%%%%%%%%%%%%%%%%%%%%%%%%%%%%%%%%%%%%%%%%%%%%%%%%%%%%%%%%%%%%%%%%%%%%
```

```
varT_non = zeros(1, length(x1));
```

```
for i = 1 : length(x1),
    cd(num2str(i));
    load center2.out;
    X = dim_coeff .* center2(:,1); Y = dim_coeff .* center2(:,2);
    varT_non(i) = coeff_long .* (std(X).^2 + std(Y).^2);
    cd(current_dir);
end
```

```
p1 = polyfit(x1, varT_non, 2)
figure;
plot(x1, varT_non, 'b*');
xlabel('\phi_t'); ylabel('{C_n^2}');
hold;
plot(x1, polyval(p1, x1), 'b-');
```

LIST OF REFERENCES

- [1] Thomas Jefferson National Accelerator Facility Office of Science Education. Specifications of the Jefferson Lab FEL.
<http://www.jlab.org/FEL/feldescrip.html>, [27 May 05].
- [2] Thomas Jefferson National Accelerator Facility Office of Science Education. Cebaf center - cavity display.
<http://education.jlab.org/sitetour/ccentercavity.html>, [27 May 05].
- [3] Laser Light from Free-Electron Laser Used for First Time in Human Surgery.
<http://www.vanderbilt.edu/News/news/dec99/nr20.html>, [27 May 05].
- [4] L'onduleur ophelie - SU_5 .
<http://www.lure.u-psud.fr/DPTS/Anneaux/Services/HMM/SU5.HTM>, [27 May 05].
- [5] R. Nave. Blue Sky and Rayleigh Scattering.
<http://hyperphysics.phy-astr.gsu.edu/hbase/atmos/blusky.html>, [27 May 05].
- [6] R. D. Hudson, Jr. *Infrared System Engineering*. Wiley & Sons, 1969.
- [7] Larry Andrews and Ronald Phillips. *Laser Beam Propagation through Random Media*. SPIE, 1998.
- [8] S. Benson et al. High Power Lasing in the IR Upgrade FEL at Jefferson Lab.
<http://www.elettra.trieste.it/fel2004/proceedings/TUCOS02/TUCOS02.pdf>, 2004.
- [9] Hugo Weichel. *Laser Beam Propagation in the Atmosphere*. SPIE Optical Engineering Press, 1990.
- [10] Brett Borden. Course notes. *PH4858 Weapons and Effects*, Fall Quarter 2005.
- [11] D. L. Fried. Dunno. *Journal of the Optical Society of America*, 56(1380), 1966.
- [12] Richard St. John. *HELCoMES User Guide*. Science Applications International Corporation, 2004.
- [13] Alan F. Stewart and Rashmi S. Shah. Diagnostic Methods for CW Laser Testing. *Proceedings of SPIE*, 5273, 2003.
- [14] W.B. Colson, C. Pellegrini, and A. Renieri. *Free Electron Laser Handbook*. Elsevier Science Publishing Company, Inc, 1990.
- [15] Fred Dylla. Private Correspondence. May 2005.

- [16] The Claremont Institute. Physics of Ballistic Missiles.
<http://missilethreat.com/overview/physics.html>, 2004 [04 Apr 05].
- [17] Missile Defense Agency. Sensors.
<http://www.acq.osd.mil/mda/mdalink/html/sensors.html>, [11 Apr 05].
- [18] Missile Defense Agency. Boost phase defense.
<http://www.acq.osd.mil/mda/mdalink/html/boost.html>, [11 Apr 05].
- [19] Missile Defense Agency. Midcourse phase defense.
<http://www.acq.osd.mil/mda/mdalink/html/midcrse.html>, [11 Apr 05].
- [20] Mobile / Tactical High Energy Laser (M-THEL) Technology Demonstration Program. *<http://www.defense-update.com/directory/THEL.htm>*, 07 May 04 [04 Jun 05].
- [21] The Claremont Institute. Missiles of the World.
<http://missilethreat.com/missiles/>, [06 Mar 05].
- [22] The Claremont Institute. Range, Accuracy, and Warheads.
<http://missilethreat.com/overview/effectiveness.html>, 2004 [04 Apr 05].
- [23] Michael H. Miklaski and Joel D. Babbitt. A Methodology for Developing Timing Constraints for the Ballistic Missile Defense System. Master's thesis, Naval Postgraduate School, 2003.
- [24] The Claremont Institute. The Materials Ballistic Missiles are Made of.
<http://missilethreat.com/overview/materials.html>, 2004 [04 Apr 05].
- [25] R. D. McGinnis et al. *Free Electron Laser Damage Studies*. Naval Postgraduate School, 2000.

INITIAL DISTRIBUTION LIST

1. Defense Technical Information Center
Ft. Belvoir, VA
2. Dudley Knox Library
Naval Postgraduate School
Monterey, CA
3. CAPT Roger McGinnis, USN
PMS-405
Washington Navy Yard, DC
4. Michael B. Deitchman
Office of Naval Research
Arlington, VA
5. Quentin Saulter
Office of Naval Research
Arlington, VA
6. Dr. Alan Todd
Advanced Energy Systems, Inc.
Princeton, NJ
7. Dr. Fred Dylla
Thomas Jefferson National Accelerator Facility
Newport News, VA
8. Dr. George Neil
Thomas Jefferson National Accelerator Facility
Newport News, VA
9. Dean, Graduate School of Engineering and Applied Sciences
Naval Postgraduate School
Monterey, CA
10. Chairman, Physics Department
Naval Postgraduate School
Monterey, CA
11. Professor William B. Colson
Naval Postgraduate School
Monterey, CA

12. Professor Robert L. Armstead
Naval Postgraduate School
Monterey, CA
13. Professor Joseph A. Blau
Naval Postgraduate School
Monterey, CA
14. Professor Peter P. Crooker
Naval Postgraduate School
Monterey, CA
15. LT Sean P. Niles, USN
Supervisor of Shipbuilding, Gulfcoast
Pascagoula, MS